Semi-Annual Technical Report
1 October 1977 to 31 March 1978

ARPA Order No.: 3291
Program Code: 7F10
Contractor: Saint Louis University
Effective Date of Contract: 1 March 1973
Contract Expiration Date: 30 September 1978
Amount of Contract: $254,459
Contract Number: F44620-73-C-0042
Principal Investigators: Brian J. Mitchell
Otto W. Nuttli
Phone: 314-535-3300, Ext. 547
Program Manager: Brian J. Mitchell
Short Title: Research in Seismology

Sponsored by

Advanced Research Projects Agency (DOD)

ARPA Order No. 3291

Monitored by AFOSR Under Contract #F44620-73-C-0042

The views and conclusions contained in this document are those of the authors and should not be interpreted as necessarily representing the official policies, either expressed or implied, of the Defense Advanced Research Projects Agency or the U.S. Government.

Research in Seismology

Semi-Annual Technical Report

Contract F44620-73-C-0042

Table of Contents:

TECHNICAL REPORT SUMMARY

Preliminary estimates of the attenuation of high frequency crustal body and surface waves have been obtained for Eurasian paths, principally for regions which are geologically young and of relatively high topographic relief. Formulas for body-wave magnitude determination and curves showing the attenuation of 1-Hz first-arrival P waves, 1-Hz Pg waves, 1-Hz Lg waves, and 0.3 to 0.5-Hz Lg waves in such regions are presented. These studies indicate that first-arrival P waves and 2 to 3-sec period Lg waves can be detected to approximately 2500 km for an m_b=4.0 earthquake if the threshold of detection is 1 millimicron. Only the 2 to 3-sec Lg waves will be seen if the threshold of detection is 10 millimicrons. For the older and geologically more stable regions of Eurasia, there are less data. These data suggest that the Attenuation of the high frequency seismic waves is less than in the geologically young regions of Eurasia, but greater than in eastern North America.

Group and phase velocities of both Rayleigh and Love waves have been obtained for numerous paths across the eastern United States. After correcting for the initial phase at the source, the data were windowed according to source-station azimuth, amplitude, and distance to obtain high quality data over paths between 400 and 2000 km in length. An inversion of these data using modern stochastic methods yields a model which is everywhere isotropic and does not require an upper-mantle low-velocity zone.

A new method using amplitude spectra of higher-mode surface waves has been developed to obtain Q models in various geologic regions. Initial results from the application of this method have been obtained for the Colorado Plateau and

Basin-and-Range province. All of the data, to date, can be explained with a model which has high Q values in the lower crust (∿2000), and values in the upper crust which are lower than those previously obtained for eastern North America.

A study of complex and simple earthquakes off the southern coast of Mexico has resulted in the observation that short-period P wave amplitudes are greatly attenuated during travel to northeastern United States stations. T/Q values between 3 and 4 would be required to explain those observations. Preliminary calculations suggest that a low-Q region above the descending slab can explain the observations. However, the possibility of defocussing due to a geometrical effect of the descending slab is also being investigated.

P-wave spectra are presented for eight earthquakes, of M_S 5.3 to 7.9. Using Brune's theory, seismic moments, source dimensions, and stress drops are estimated from the long-period level of the spectrum and the corner period. The m_b:M_S values for six of the eight earthquakes satisfy the relation proposed by Geller.

TENTATIVE VALUES OF ATTENUATION OF HIGH-FREQUENCY SEISMIC WAVES AT REGIONAL DISTANCES IN EURASIA

by

Otto W. Nuttli

INTRODUCTION

Detection, location, discrimination and yield determinations of underground nuclear explosions all require a knowledge of the attenuation of the amplitudes of seismic phases with distance. If measurements of these phases are made at regional distances (less than about 2500 km) then the wave attenuation will in general vary with geologic region, as the structure of the earth's upper crust varies laterally. For example, Evernden (1967) has shown that the P phases (Pn, Pg and P refracted in the upper mantle) are much more strongly attenuated in the western than in the eastern United States. Nuttli (1973) showed that short-period Lg waves in eastern North America (east of Rocky Mountain front) have a low attenuation, whereas those for wave paths west of the front are severely attenuated. On the basis of those attenuation studies North America can be divided into two provinces, namely a Type-A region of relatively flat topography and old surficial rocks and a Type-B region of more rugged topography and young surficial rocks.

Physiographically, Eurasia also may be divided into a Type-A and a Type-B region (Figure 1). Type-A includes France, Germany, Poland and the Soviet Union east to about 90°E and 120°E longitude. Type-B includes the Mediterranean countries, Iran, Afghanistan, Pakistan, China and the eastern part of the Soviet Union. At present it is not known how the Ural Mountains or seas such as the Caspian, Black or Baltic would affect the propagation of 1-Hz Lg waves, or of crustal body phases or somewhat longer period surface waves.

DATA

The WWSSN stations SHI (Shiraz, Iran), MSH (Mashad, Iran), KBL (Kaboul, Afghanistan), and QUE (Quetta, Pakistan) provided the basic data for this study. The location of the stations is shown in Figure 1, from which it can be seen that SHI, KBL and QUE are in Type-B regions and MSH is near the border of Type-A and Type-B regions. For the present study only the short-period, vertical-component seismograms were used. Future studies will also make use of short-period horizontal-component seismograms.

From the Bulletin of the International Seismological Centre (BISC) earthquakes were selected which were within 2500 km distance of the stations SHI, MSH, KBL and QUE and which had paths through Type-A or Type-B structure. The former were restricted to events in the Soviet Union to the north of MSH. The latter consisted of earthquakes in Iran, Afghanistan, Tadzhikistan, Caucasus, Turkey and Hindu Kush. For the period of study, August through December 1971, the magnifications of the short-period vertical seismographs at 1-sec period were 50,000 at SHI, 6,250 or 12,500 at MSH, 200,000 or 400,000 at KBL and 200,000 at QUE. Table 1 gives the dates, locations and body-wave magnitudes of the events studied.

Zero-to-peak amplitudes and periods were read for the phases P, Pg and Lg, all from the vertical-component seismograms. For Lg the maximum sustained motion (defined as the largest amplitude equalled or exceeded by 3 cycles of motion), rather than the peak amplitude, was read. All amplitudes were equallized to a body-wave magnitude of 5.0, using the m_b value given by the ISC. The amplitudes were plotted on log-log paper as a function of epicentral distance for a particular wave type of a given period.

Figure 2 is an example of 1-sec Lg wave motion from Iranian earthquakes recorded at SHI and MSH, the Iranian stations. For these earthquakes the paths are through Iran, which is of Type-B structure. The data are fit reasonably well by theoretical time-domain surface wave curves with a coefficient of sbsorption between 0.004 and 0.005 km^{-1}. One can approximate these curves over the distance range 200 to 800 km by the dashed-line curve in Figure 2, which gives the equations

$$m_b = -1.73 + 2.56 \log \Delta + \log A \qquad \text{for } 200 \text{ km} \leq \Delta \leq 800 \text{ km}$$

and over the distance range 800 to 1500 km by

$$m_b = -9.60 + 5.25 \log \Delta + \log A \qquad \text{for } 800 \text{ km} \leq \Delta \leq 1500 \text{ km}$$

where

Δ is epicentral distance in kilometers

A is maximum sustained zero-to-peak amplitude of 1.0 sec ($\pm$ 0.3 sec) vertical-component Lg ground motion, in microns. The attenuation of 1-Hz Lg waves in Iran is so severe that these waves will not be measurable beyond 1500 km for an $m_b = 5.0$ event. Thus no m_b formula is given for greater distances.

Figure 3 presents the attenuation data for 1-Hz Lg waves for Type-B Eurasian paths for a variety of source regions. As it be expected, the data scatter more than that of Figure 2. However, for the most part the data are bounded by theoretical curves of $\gamma = 0.003$ and 0.006 km^{-1}. The dashed line, which lies approximately midway between the $\gamma = 0.003$ and 0.006 km^{-1} curves, yields the equations

$$m_b = -2.31 + 2.68 \log \Delta + \log A \qquad \text{for } 400 \text{ km} \leq \Delta \leq 700 \text{ km}$$

$$m_b = -8.97 + 5.00 \log \Delta + \log A \qquad \text{for } 700 \text{ km} \leq \Delta \leq 1500 \text{ km}.$$

Figure 4 shows the attenuation of 2 to 3-sec period Lg waves for Type-B Eurasian paths. Most of the data points lie between the theoretical curves of $\gamma = 0.003$ and $0.005\ km^{-1}$. A median curve, shown by the dashed line, gives the equations

$$m_b = -8.30 + 4.45 \log \Delta + \log A \quad \text{for} \quad 700\ km \leq \Delta \leq 1200\ km$$

$$m_b = -16.90 + 7.20 \log \Delta + \log A \quad \text{for} \quad 1200\ km \leq \Delta \leq 2000\ km.$$

Data for Lg waves traveling through Type-A Eurasian structure are few for the time interval studied. There were just two earthquakes and one underground explosion, as shown in Figure 5. The two earthquake data points can be joined by a theoretical attenuation curve of $\gamma = 0.002\ km^{-1}$. As expected, the amplitude of the nuclear explosion ground motion is considerably less than that predicted by the earthquake attenuation curve.

No magnitude formulas for 1-Hz Lg wave amplitudes in a Type-A Eurasian structure will be given, as the data are too few to justify presenting them.

The 1-Hz Pg amplitude data for Type-B and Type-A Eurasian paths are shown in Figures 6 and 7, respectively. The former can be fit by a straight line of slope -2.86, with a standard deviation of 0.3 magnitude units, as seen in Figure 6. For comparison purposes the two data points for a Type-A path are shown along with the attenuation curve for a Type-B path in Figure 7. From Figure 6 the following magnitude formula based on the amplitude of the vertical component of 1-Hz Pg motion for Type-B paths can be derived

$$m_b = -2.40 + 2.86 \log \Delta + \log A \quad \text{for} \quad 300\ km \leq \Delta \leq 1000\ km.$$

Figure 8 is a plot of the amplitudes of 1-Hz P waves (Pn or P refracted through the upper mantle) for Type-B paths through Eurasia, equalized to $m_b = 5.0$. The data were divided into 200-km intervals, and the logarithmic average

determined for each interval. The average values are shown by solid lines. The dashed lines indicate the standard deviations. In general the standard deviations are large, which probably results from the fact that no correction was made for unequal azimuthal radiation and for the fact that there may be lateral variations within the Type-B region.

From Figure 8 a tentative P-wave calibration function, log $A_o(\Delta)$, can be given to be used with the formula

$$m_b = \log A + \log A_o(\Delta)$$

where A is zero-to-peak, vertical-component ground motion of the Pn or P wave in microns at distances of 400 to 2500 km. The values of log A_o are given in Table 2.

DISCUSSION AND CONCLUSIONS

This report presents tentative findings for the attenuation and excitation of P, Pg and Lg waves (vertical component) for Eurasian paths. Much more data need to be accumulated to minimize the effects of unequal azimuthal radiation and to subdivide Eurasia into different tectonic provinces. However, the present data are adequate to give some order-of-magnitude estimates of the ground motion to be expected for various magnitude events in Type-A and Type-B Eurasian regions.

The data can be summarized in a table (Table 3), which presents the vertical-component ground motion for specific waves for Type-A and Type-B structures. An earthquake of body-wave magnitude equal to 4.0 was arbitrarily selected for these calculations, because it corresponds to a low-yield explosion. Scaling can be readily carried out for other m_b values.

The values in Table 3 are tentative, and will be revised as more data are gathered. In particular, much more data for Type-A structure are needed. Also,

as can be seen from the graphs, the scatter in amplitude values is large, sometimes as great as an order of magnitude. Thus the numerical values in Table 3 are to be taken as average values.

Consider first a 1 millimicron threshold of detection, which is probably an optimistic one. For an m_b = 4.0 earthquake in Type-A structure the 1-Hz Lg wave could be seen as far as 2500 km, but in Type-B structure only to 1500 km. The 2 to 3 sec Lg wave in Type-B structure could be seen to 2100 km, and the 1-Hz Pg in the same structure to 1900 km. The 1-Hz P wave in Type-B structure could be seen to 2500 km.

If the threshold of detection is taken to be 10 millimicrons, then for an m_b = 4.0 earthquake the 1-Hz Lg wave could be seen to 1500 km for Type-A structure and to 1000 km for Type-B structure. For Type-B structure the 2 to 3 sec period Lg wave could be seen to 1500 km, the 1-Hz Pg to 900 and the 1-Hz P would in general be too small to be observed at all regional distances.

There are just 3 data points for 1-Hz P waves in Type-A structure, 2 for earthquakes and 1 for an underground explosion, all recorded at MSH. They lie within the scatter of the Type-B data, suggesting that there is no appreciable difference in P-wave attenuation for the two regions. This is a surprising result, which may just be due to the insufficiency of data. From Figure 7 we can see that the 1-Hz Pg waves in Type-A regions appear to have approximately 5 times the amplitude of similar waves in Type-B regions.

Keeping in mind reservations relating to the incompleteness of the data, particularly for Type-A Eurasian structure, we can make the following preliminary conclusions:

1) 1-Hz Lg and Pg waves can be utilized in Type-A (geologically old, low relief) regions to detect earthquakes down to m_b = 4.0 for distances as large

as 2500 km if the threshold of detection is 1 millimicron. If the threshold of detection is 10 millimicrons, the corresponding maximum distance is 1500 km.

2) 1-Hz P (Pn or P refracted through the upper mantle) and 2 to 3 sec period Lg waves are best suited to detect earthquakes in Type-B (geologically young, high relief) regions if the threshold of detection is 1 millimicron. The P wave will be seen to 2500 km and the 2 to 3 sec Lg wave to 1900 km for an m_b = 4.0 earthquake. However, the P-wave amplitude will be small, and easily masked by noise. If the detection threshold is changed to 10 millimicrons an m_b = 4.0 earthquake will not produce identifiable P waves at regional distances.

3) 1-Hz Lg waves in Eurasian Type-B regions are strongly attenuated, similar to the western United States.

REFERENCES

Evernden, J.F. "Magnitude determinations at regional and near-regional distances in the United States", Bull. Seism. Soc. Am., 57, 591-639, 1967.

Nuttli, O.W. "Seismic wave attenuation and magnitude relations for eastern North America", J. Geophys. Res., 78, 876-885, 1973.

TABLE 1

EVENTS STUDIED

Date	Origin Time (UT)	Lat(°N)	Long(°E)	h (km)	m_b(ISC)
07 Aug 71	17 07 25	38.87	29.91	20	4.6
09 Aug 71	02 54 35	36.27	52.81	12	5.2
22 Aug 71	17 54 16.7	30.08	50.75	51	4.9
26 Aug 71	06 55 08	30.06	50.83	42	4.7
27 Aug 71	05 20 15.3	30.12	50.73	56	4.8
28 Aug 71	16 34 42.9	37.75	56.16	33	4.8
01 Oct 71	16 27 47	38.72	69.74	21	4.9
05 Oct 71	18 31 18.7	27.24	55.88	44	5.1
06 Oct 71	23 43 23.1	37.72	72.19	38	4.8
14 Oct 71	21 55 52.9	36.50	71.15	82	5.0
15 Oct 71	14 19 32.0	37.33	54.59	41	4.6
15 Oct 71	16 22 12.3	37.02	71.87	156	4.9
15 Oct 71	17 08 08.1	41.35	48.58	54	4.8
16 Oct 71	06 11 38.6	37.13	71.36	98	4.6
28 Oct 71	13 30 56.4	41.88	72.35	15	5.4
08 Nov 71	03 06 34	27.04	54.57	11	5.6
09 Nov 71	00 16 56	26.89	54.52	9	4.7
13 Nov 71	15 47 44	11.03	39.71	39	5.1
18 Nov 71	07 31 33	38.44	66.78	27	5.2
19 Nov 71	01 00 01.9	41.87	72.35	39	4.9
09 Dec 71	01 42 32	27.28	56.42	24	5.3
15 Dec 71	15 24 58.3	30.24	50.57	51	5.1
20 Dec 71	01 29 14	41.23	48.38	2	5.1
20 Dec 71	01 41 04	41.14	48.40	28	5.1
20 Dec 71	07 53 08	41.19	48.45	4	4.8
20 Dec 71	23 27 43.7	28.32	57.19	84	5.0
21 Dec 71	09 54 52	35.57	74.28	15	5.0
22 Dec 71	06 59 56.5 Expl.	47.90	48.07	0	6.0
27 Dec 71	20 59 39.3	34.98	73.02	55	5.2
29 Dec 71	21 12 40.0	29.54	52.74	34	4.9

TABLE 2

CALIBRATION FUNCTION FOR P WAVES

Δ (km)	log A_o
400 - 600	6.45
600 - 800	5.84
800 - 1000	6.18
1000 - 1200	6.21
1200 - 1400	6.52
1400 - 1600	6.26
1600 - 1800	6.61
1800 - 2000	6.31
2000 - 2200	6.53
2200 - 2400	6.02

TABLE 3

WAVE AMPLITUDES FOR AN EURASIAN m_b = 4.0 EARTHQUAKE

	Type-A	Type-B			
Δ (km)	1-Hz Lg (μ)	1-Hz Lg (μ)	3-sec Lg (μ)	1-Hz Og (μ)	1-Hz P (μ)
500	0.21	0.12	--	0.047	0.004
700	0.10	0.051	0.46	0.019	0.015
900	0.055	0.016	0.15	0.009	0.007
1100	0.033	0.006	0.068	0.006	0.006
1300	0.020	0.0025	0.027	0.004	0.003
1500	0.011	0.001	0.010	0.0025	0.006
1700	0.007	*	0.005	0.002	0.002
1900	0.004	*	0.002	0.001	0.005
2100	0.003	*	0.001	*	0.003
2300	0.0015	*	*	*	0.010
2500	0.001	*	*	*	--

*Ground motion less than 1 millimicron

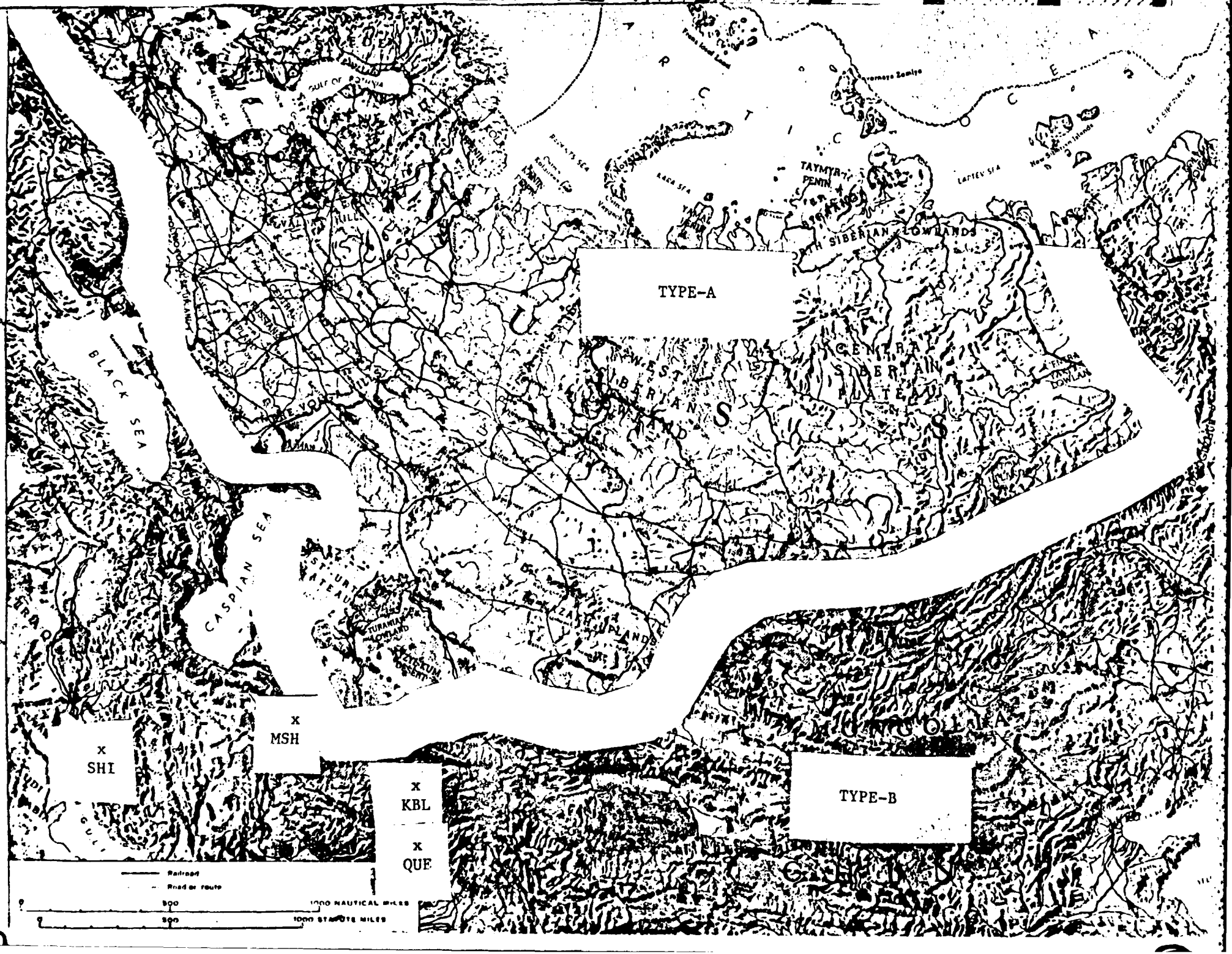
TYPE-A
TYPE-B
SHI
MSH
KBL
QUE
BLACK SEA
CASPIAN SEA
Railroad
Road or route
500
1000 NAUTICAL MILES
500
1000 STATUTE MILES

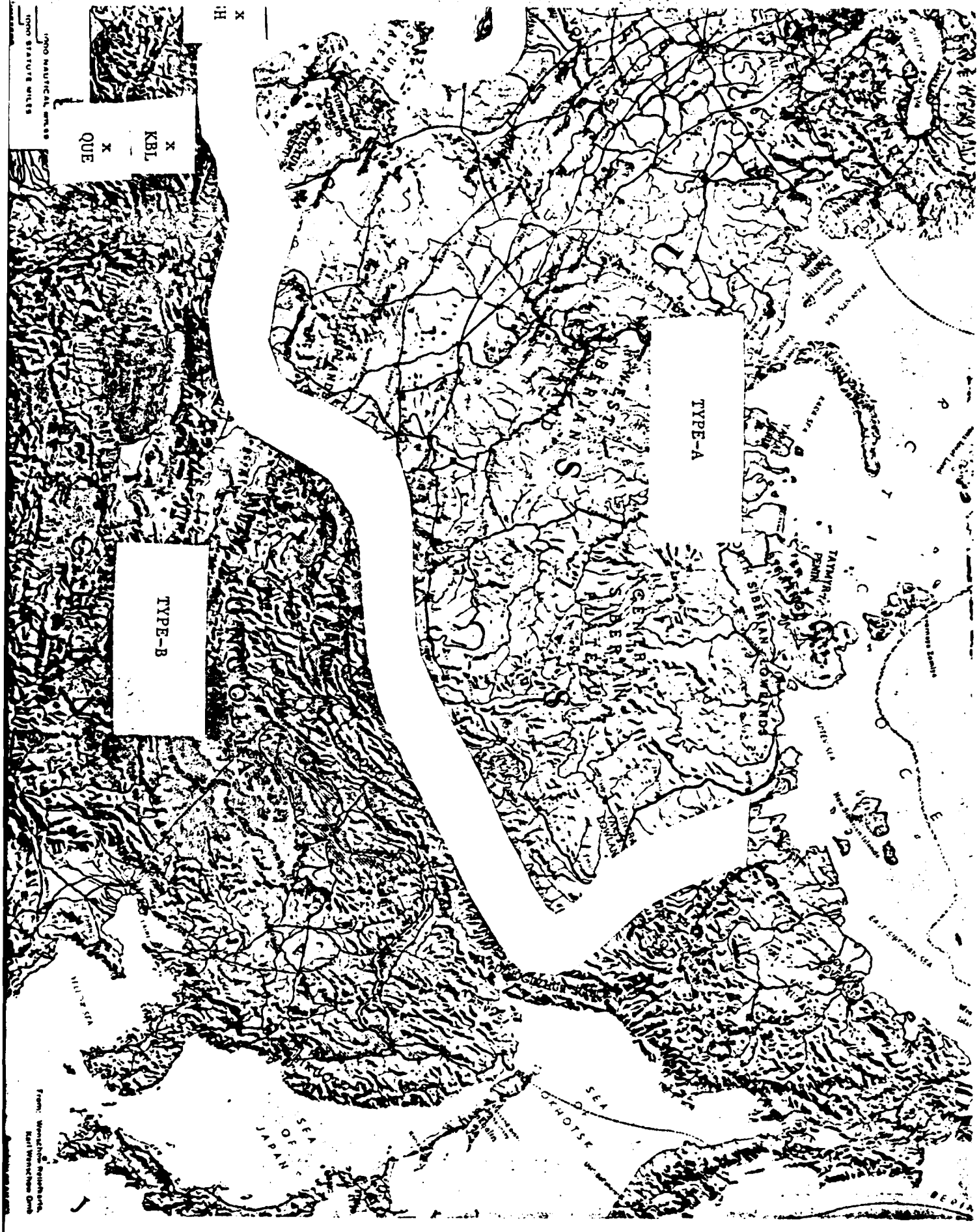

Figure 1. Type-A and Type-B Physiographic Regions of Eurasia and Location of Seismograph Stations Used in the Study

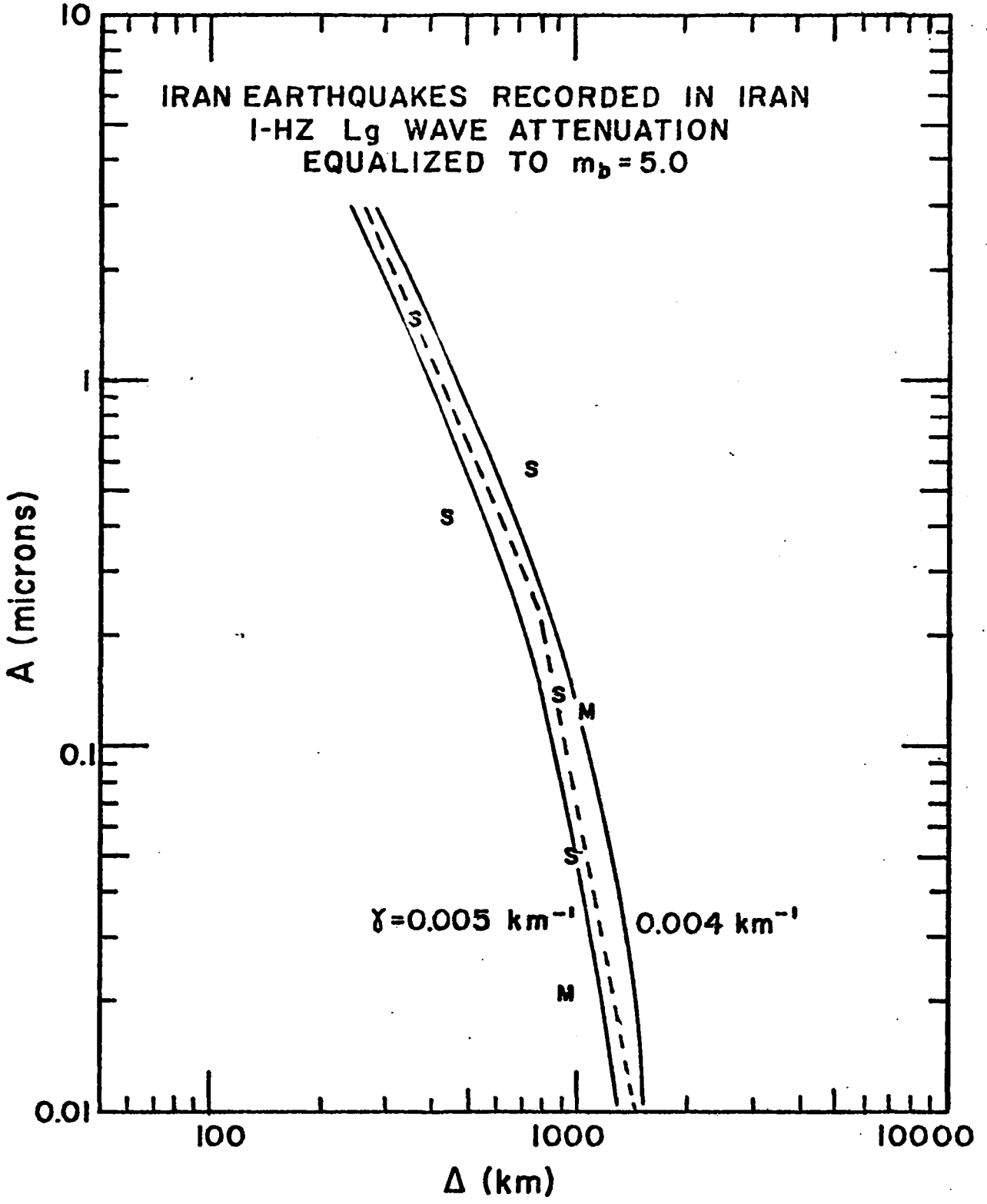

Figure 2. Attenuation of 1-Hz Lg waves (Z-component) for Iran earthquakes recorded at SHI (S) and MSH (M), both in Iran. The dashed line is an approximation to the attenuation relation which is used for deriving magnitude formulas.

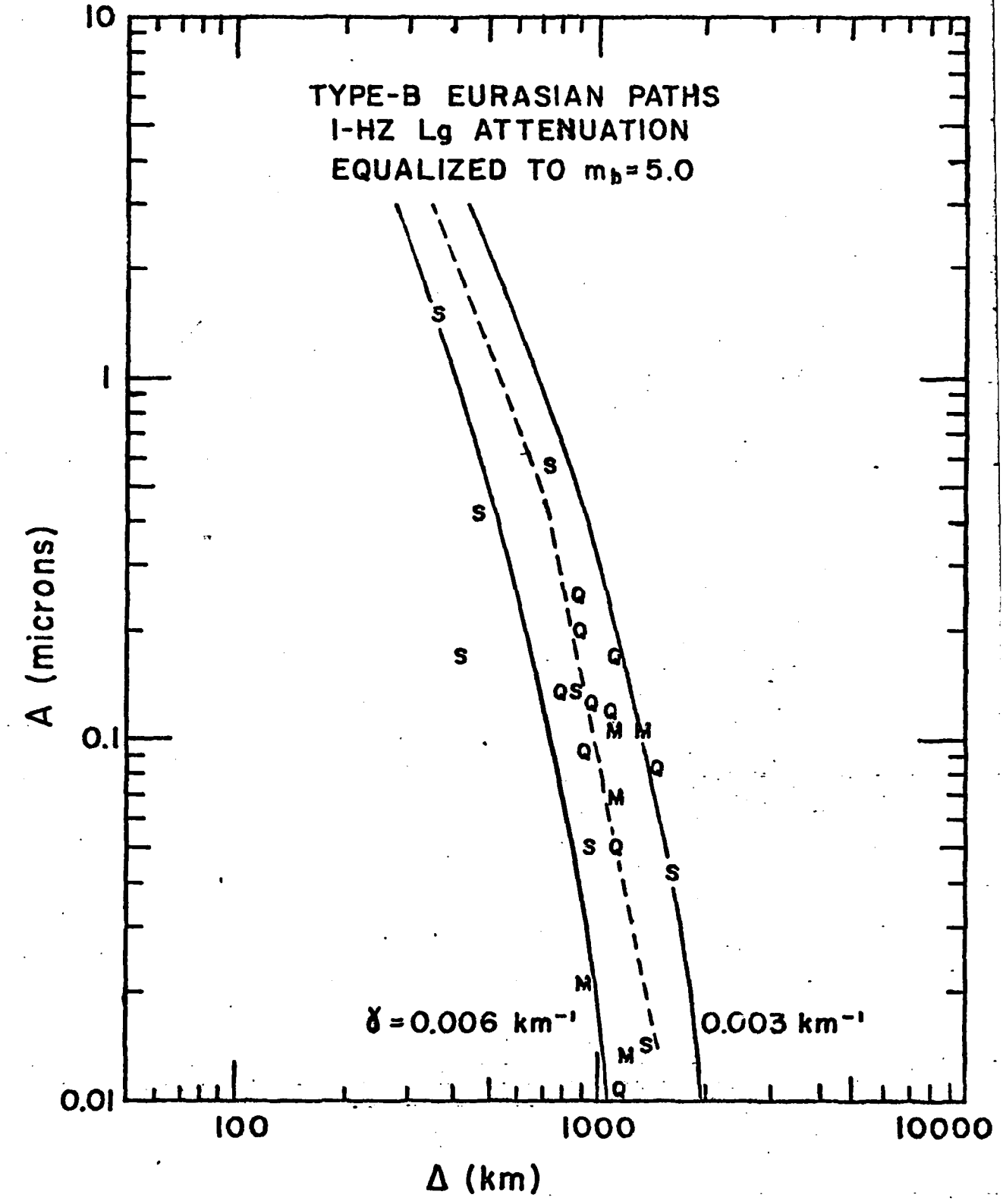

Figure 3. Attenuation of 1-Hz Lg waves (Z-component) for Type-B paths to SHI (S), QUE (Q) and MSH (M). The dashed line is an approximation to the attenuation relation which is used for deriving magnitude formulas.

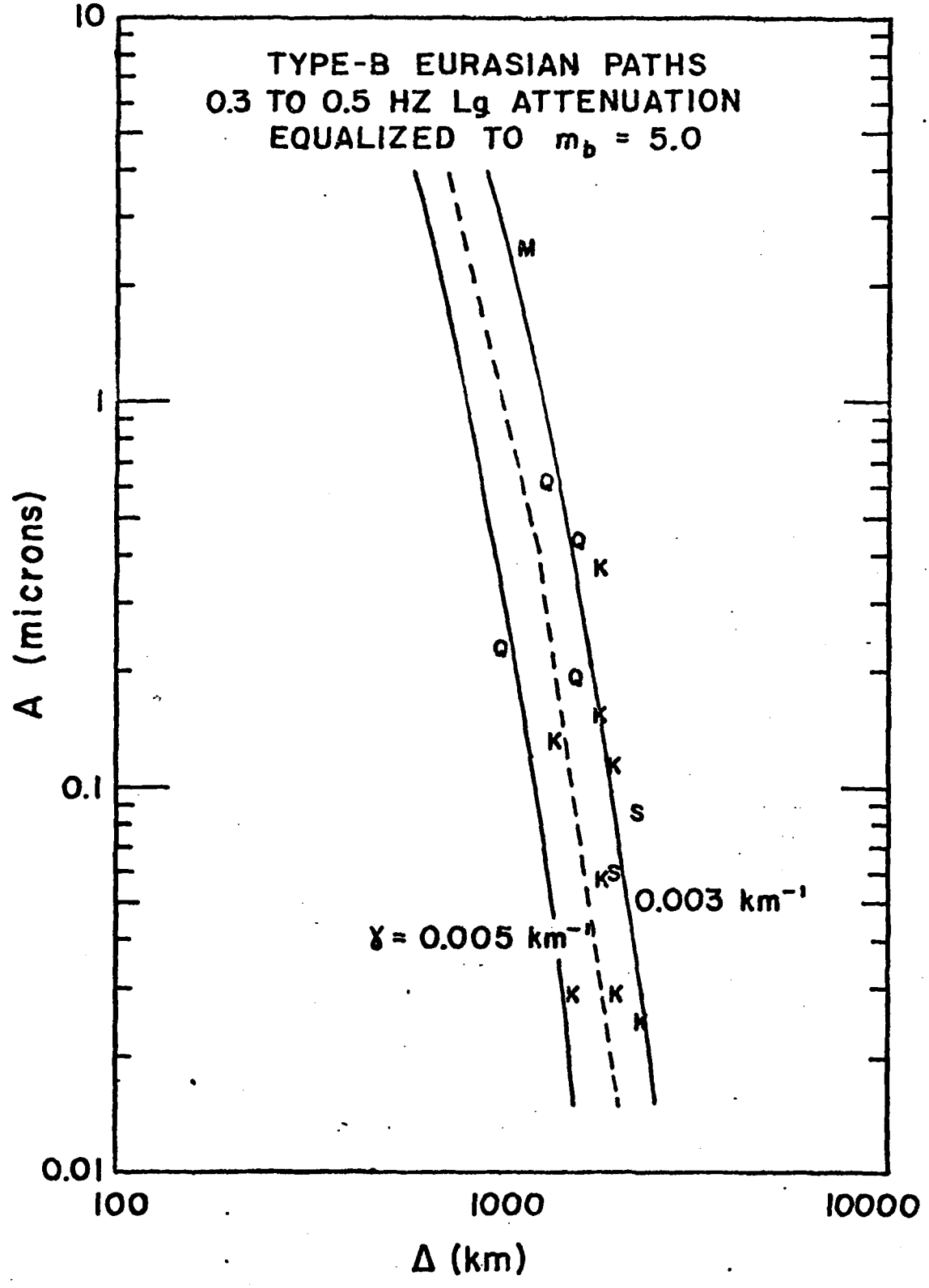

Figure 4. Attenuation of 2 to 3-sec period Lg waves (Z-component) for Type-B paths to SHI (S), QUE (Q), MSH (M) and KBL (K). The dashed line is an approximation to the attenuation relation which is used for deriving magnitude formulas.

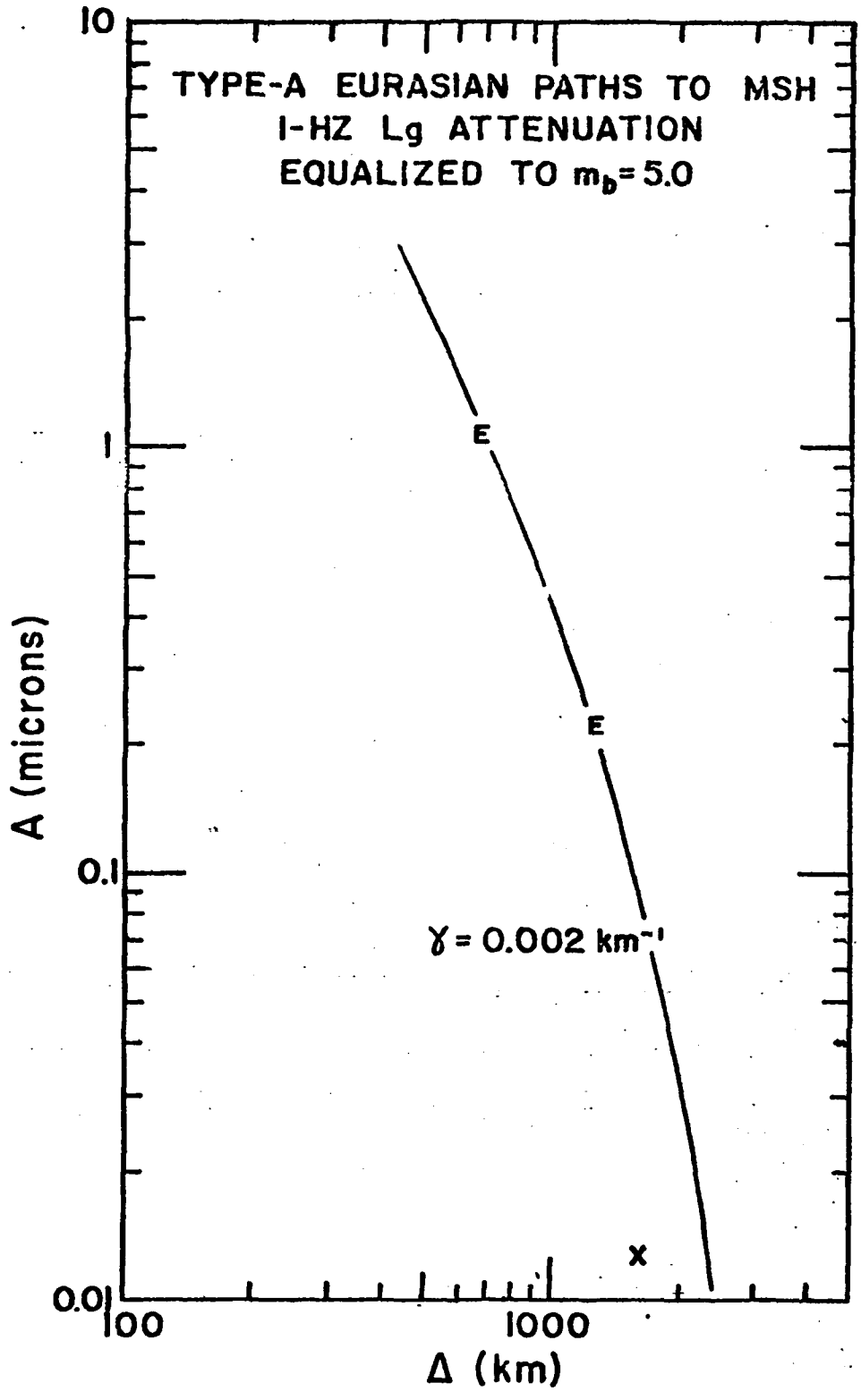

Figure 5. Attenuation of 1-Hz Lg waves (Z-component) for Type-A paths to MSH. E indicates earthquakes and X underground nuclear explosion.

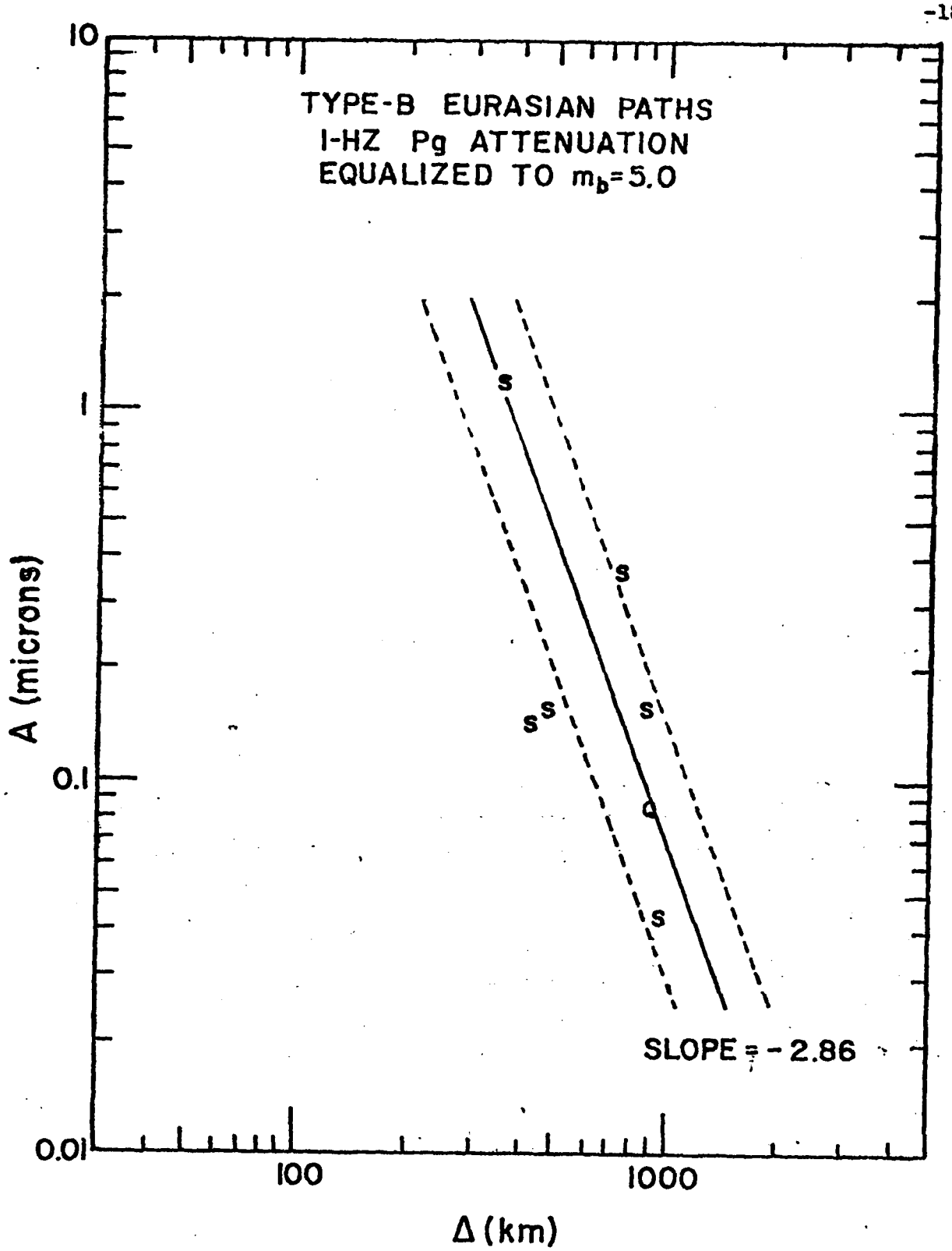

Figure 6. Attenuation of 1-Hz Pg waves (Z-component) for Type-B paths to SHI (S) and QUE (Q). The solid line is an average straight-line curve. The dashed lines are offset from the solid-line curve by one standard deviation.

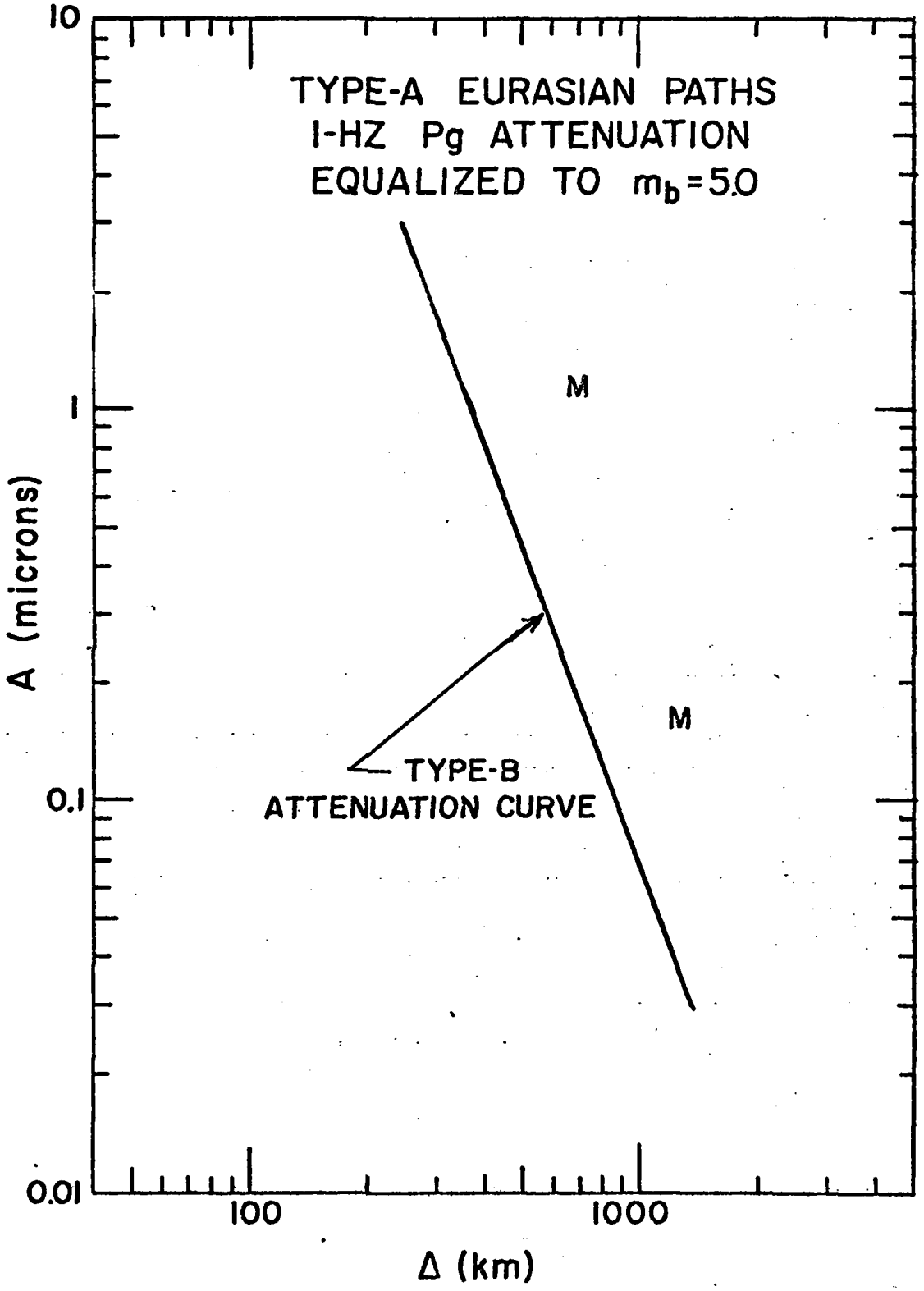

Figure 7. Amplitude of 1-Hz Pg waves (Z-component) for Type-A paths to MSH (M) compared to amplitudes and attenuation for a Type-B path.

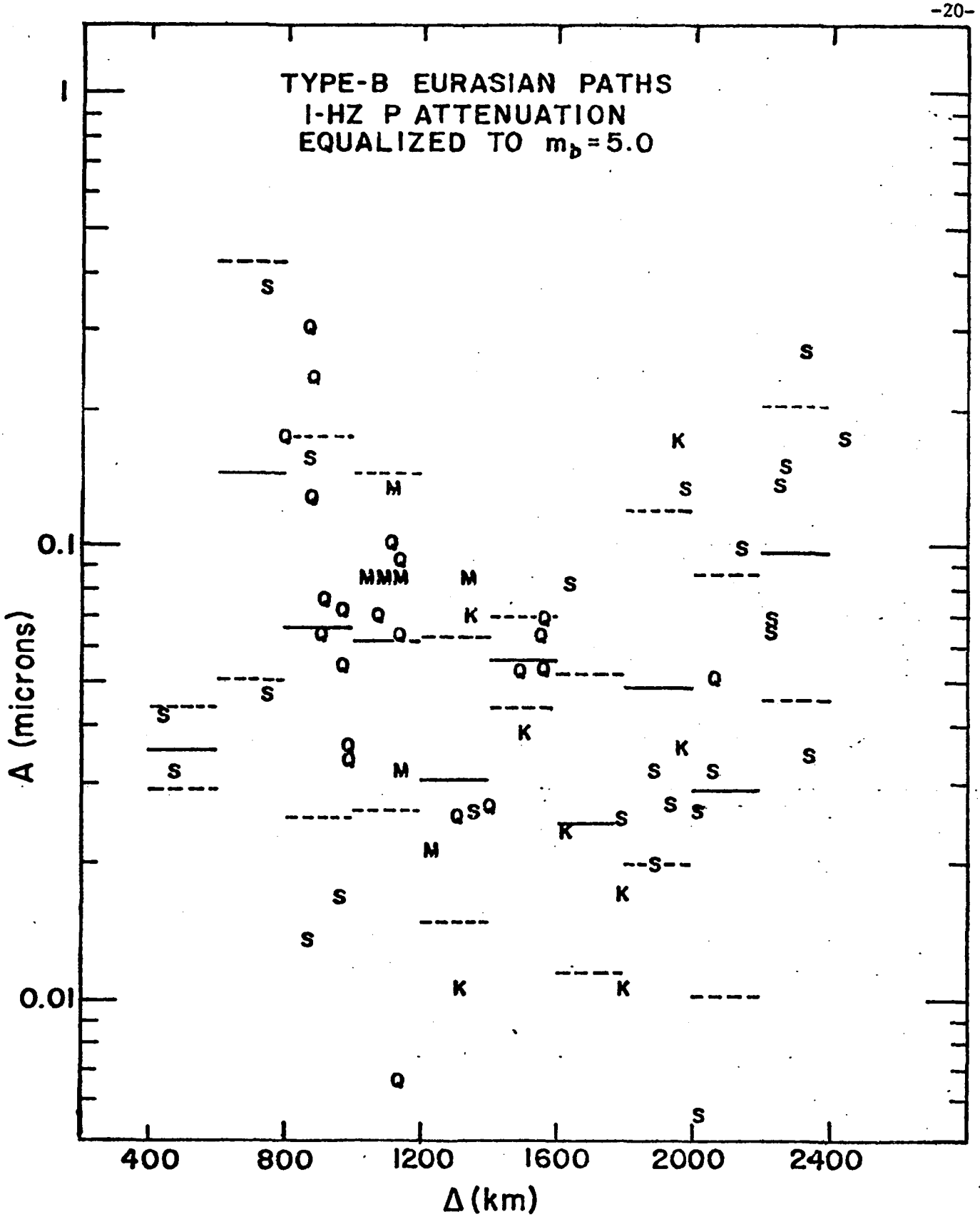

Figure 8. Attenuation of 1-Hz P (Pn and P refracted through upper mantle, Z-component) for Type-B paths to SHI (S), QUE (Q), MSH (M) and KBL (K). The solid-line curves represent logarithmic averages over 200 km intervals. The dashed lines are offset from the solid-line curves by one standard deviation.

SURFACE-WAVE DISPERSION IN THE EASTERN UNITED STATES

by

Brian J. Mitchell

We are currently implementing methods to investigate higher-modes and the effect of crustal and upper-mantle Q values upon their amplitudes (see the following section of this report). Among the important preliminary information necessary for such studies, is a reasonably good knowledge of the shear wave velocity structure in the region of study. The central United States is one region where the method will be applied, since hat region can be considered to be representative of relatively stable continental interior regions in various parts of the world.

McEvilly (1964) determined shear velocity models for the central United States using phase velocities obtained from observations at stations in Rolla, Missouri, Manhattan, Kansas, Bloomington, Indiana, and Dubuque, Iowa. In order to fit both Rayleigh and Love wave observations, McEvilly found it necessary to invoke a model which was anisotropic in its elastic properties in the upper mantle and, possibly also, in the lower crust. He cautioned, however, that it was possible that the Love wave observations could be adversely affected by higher-mode interference, or that a more complicated isotropic model might explain all of the data.

A large body of group velocity data is now available for the eastern and central United States. These were obtained as a by-product of studies of earthquake fault-plane solutions in the central United States (Herrmann, 1974). The group velocities were determined by the multiple-filter method (Dziewonski,

et al., 1969). Application of that method permits us to avoid higher-mode interference, since spectral amplitudes associated with the fundamental mode and higher modes are usually separated by group velocity or period. The group velocities were corrected for group delays at the source (Knopoff and Schwab, 1968). This correction is especially important for epicenter-station paths which are relatively short.

The available data (Figure 1) were taken from numerous paths across both eastern and western North America. Factors which produce the great scatter in this data are (1) regional differences in group velocity, (2) low signal-noise ratios associated with some of the data, (3) possible misidentification of energy maxima, and (4) possible inaccuracies in the obtained fault-plane solution which would yield the incorrect initial phase at the source.

I have windowed the data in several ways in an attempt to reduce the scatter in the group velocities of Figure 1. First, I have restricted the paths used to lie at azimuths between 350° and 130° (Figure 2). A model obtained from these data will predominantly represent the crust and upper mantle for a region of the United States, south of the Great Lakes and extending to the east coast. Slower group velocities corresponding to paths to the west and south have been removed. Second, I have required that all data have spectral amplitudes which are at least one-fifth as large as the maximum amplitude for that event and period. It is hoped that all data with a low signal-noise ratio will be removed in this way. Third, all data for paths which are less than 400 km long have been removed. This will minimize any inaccuracies associated with an incorrect initial phase due to an erroneous fault-plane solution for the earthquake. Finally, I have removed any isolated data points which depart greatly from the mean at any period.

Such points, after removing low amplitude data, presumably correspond to amplitude maxima which have been erroneously identified as fundamental Love or Rayleigh wave energy.

The windowed Love and Rayleigh wave group velocity data appear in Figure 3. It is clear that the above-mentioned windowing procedures have significantly decreased the scatter which was apparent in Figure 1. Phase velocities were also determined (by the single-station method) using the better seismograms pertaining to the data of Figure 3. These phase velocities are about the same as those obtained by McEvilly (1964), both for Love waves and Rayleigh waves.

The average group and phase velocities, along with their standard deviations are plotted in Figure 4 and compared with theoretical curves for three models from McEvilly (1964). The best-fitting model is one which is anisotropic, both in the upper mantle and lower crust. It fits both sets of phase velocities quite well, and also shows reasonable agreement with the Rayleigh wave group velocities, except at the shortest periods. It fails, however, to even come close to fitting the Love wave group velocities.

It is now possible, due to the development of modern inversion methods (Backus and Gilbert, 1970), to invert sets of data directly, rather than use the trial-and-error methods which were available to McEvilly (1964). These methods allow us to investigate a wider range of models than had been previously possible.

I first attempted to obtain an isotropic model which might fit all of the data, phase and group velocities for both Rayleigh and Love waves. The fit to the data achieved by obtaining such a model is shown in Figure 5. The fit is reasonably good, failing to fall within the standard deviation bars for only one data point. Separate inversions of the Love- and Rayleigh-wave data were also

performed in order to see if a significant improvement in the fit to the data could be achieved. Although some improvement was obtained, the results indicate that anisotropy is not required in either the lower crust of upper mantle of the eastern United States.

The models obtained from these inversions are shown in Figure 6. The differences in the dispersion results for the present study and that of McEvilly (1964) appear to be due to the following features of the models in Figure 6 which were not present in the earlier model: (1) A low-velocity sedimentary layer is required to fit the short-period group velocities, (2) lower velocities are present in the upper crust, (3) the lower crust may include a decrease in velocity with depth, and (4) a low-velocity zone, although possible, is not required by the data. I plan to investigate item (3) further by computing multi-mode synthetic surface wave seismograms for models with, and without, a decrease in shear wave velocity in the lower crust.

Figure 7 presents the resolving kernels associated with the models of Figure 6. It is clear that the resolution is reasonably good to depths as great as those in the shallow portion of the upper mantle. At greater depths the resolution becomes poorer.

REFERENCES

Dziewonski, A.M., S. Bloch, and M. Landisman, A technique for the analysis of transient seismic signals, Bull. Seism. Soc. Am., 59, 427-444, 1969.

Herrmann, R.B., Surface Wave Generation by Central United States Earthquakes, Ph.D. Thesis, 262 pp., St. Louis Univ., St. Louis, Mo., 1974.

Knopoff, L., and F.A. Schwab, Apparent initial phase of a source of Rayleigh waves, J. Geophys. Res., 73, 755-760, 1968.

McEvilly, T.V., Central U.S. crust-upper mantle structure from Love- and Rayleigh-wave phase velocity inversion, Bull. Seism. Soc. Am., 54, 1997-2015, 1964.

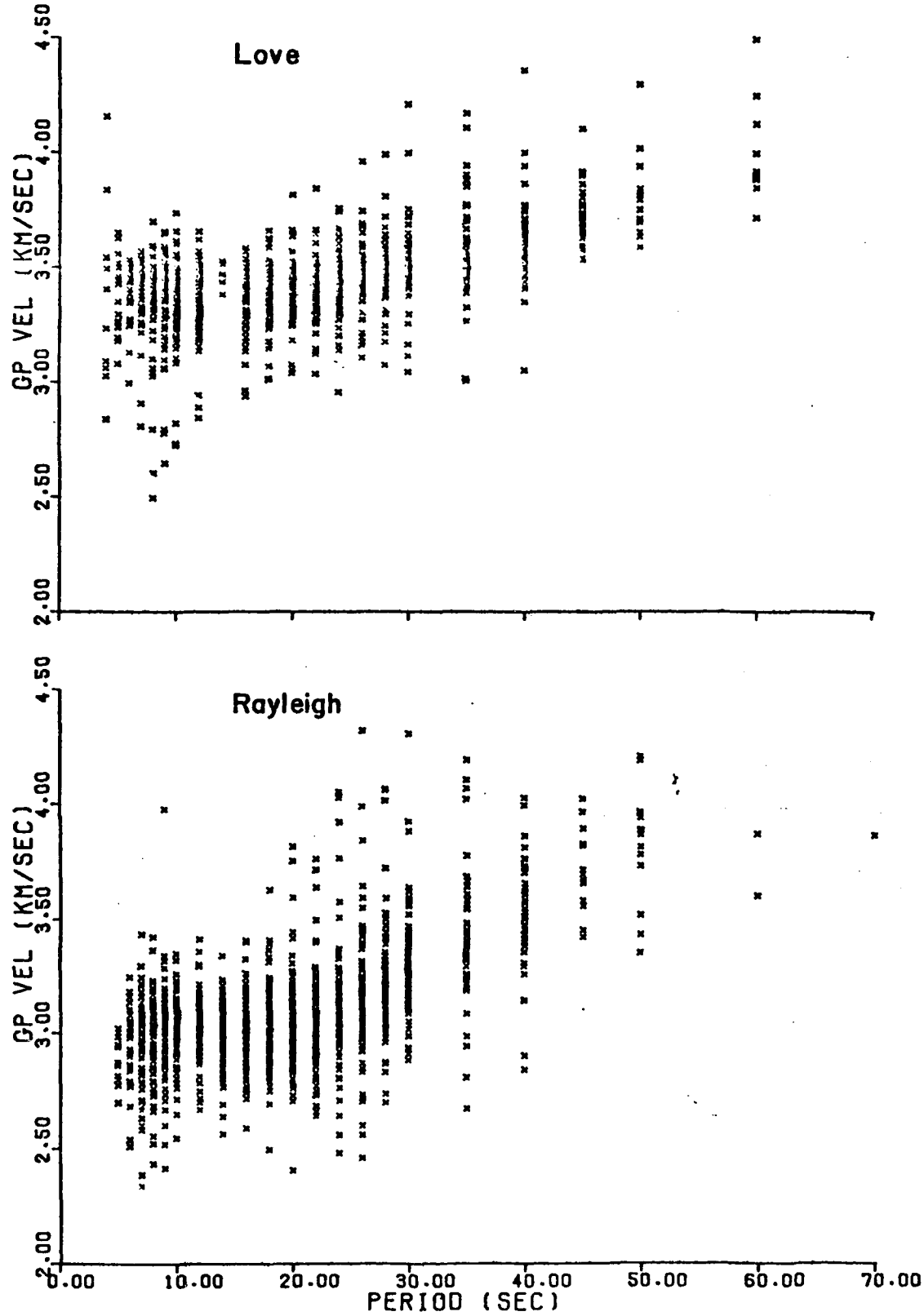

Figure 1. Group velocity values obtained for numerous paths across North America from central United States earthquakes.

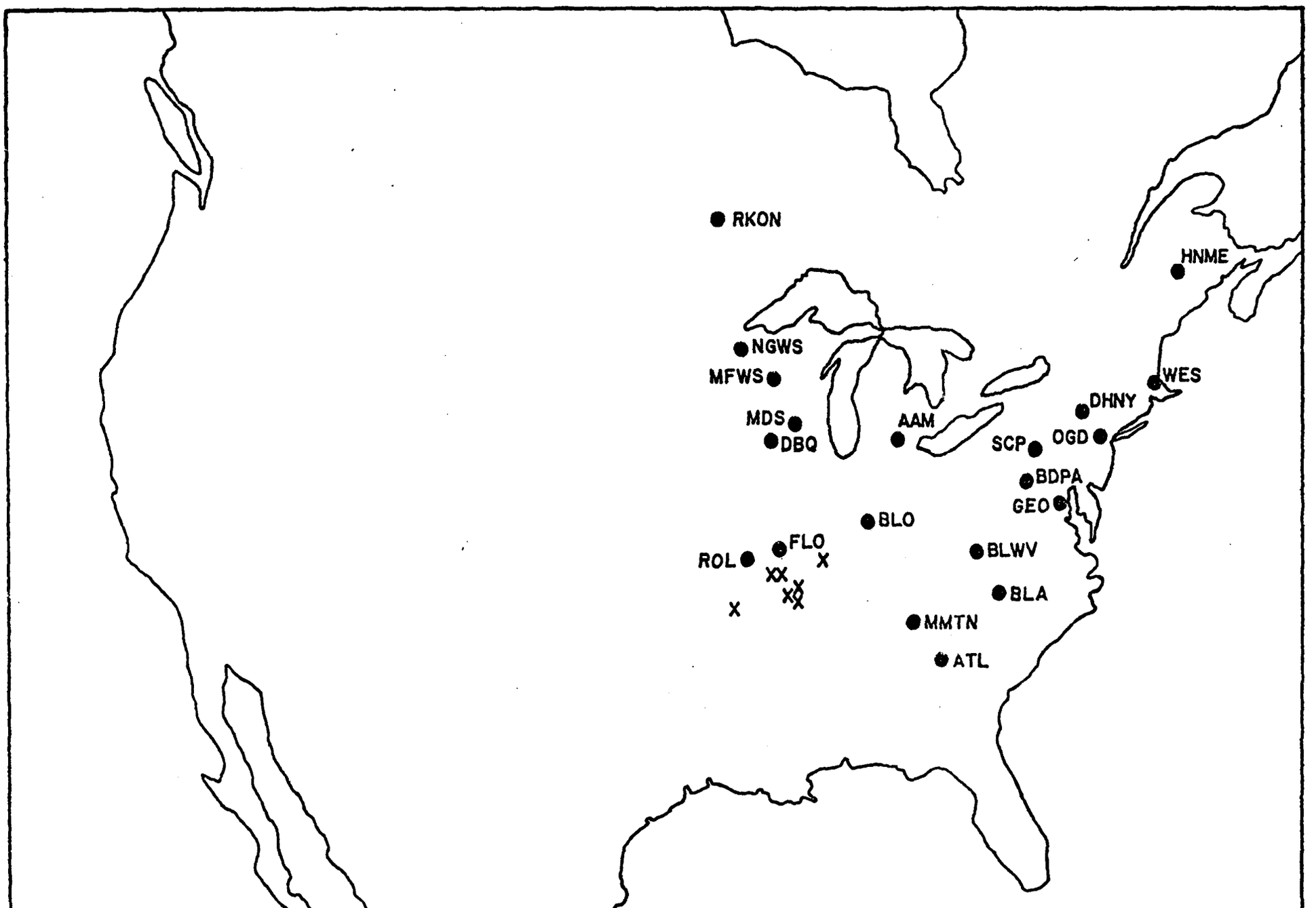

Figure 2. Map of the United States showing the locations of earthquakes with known fault-plane solutions in the central United States and stations for which windowed group velocities were obtained.

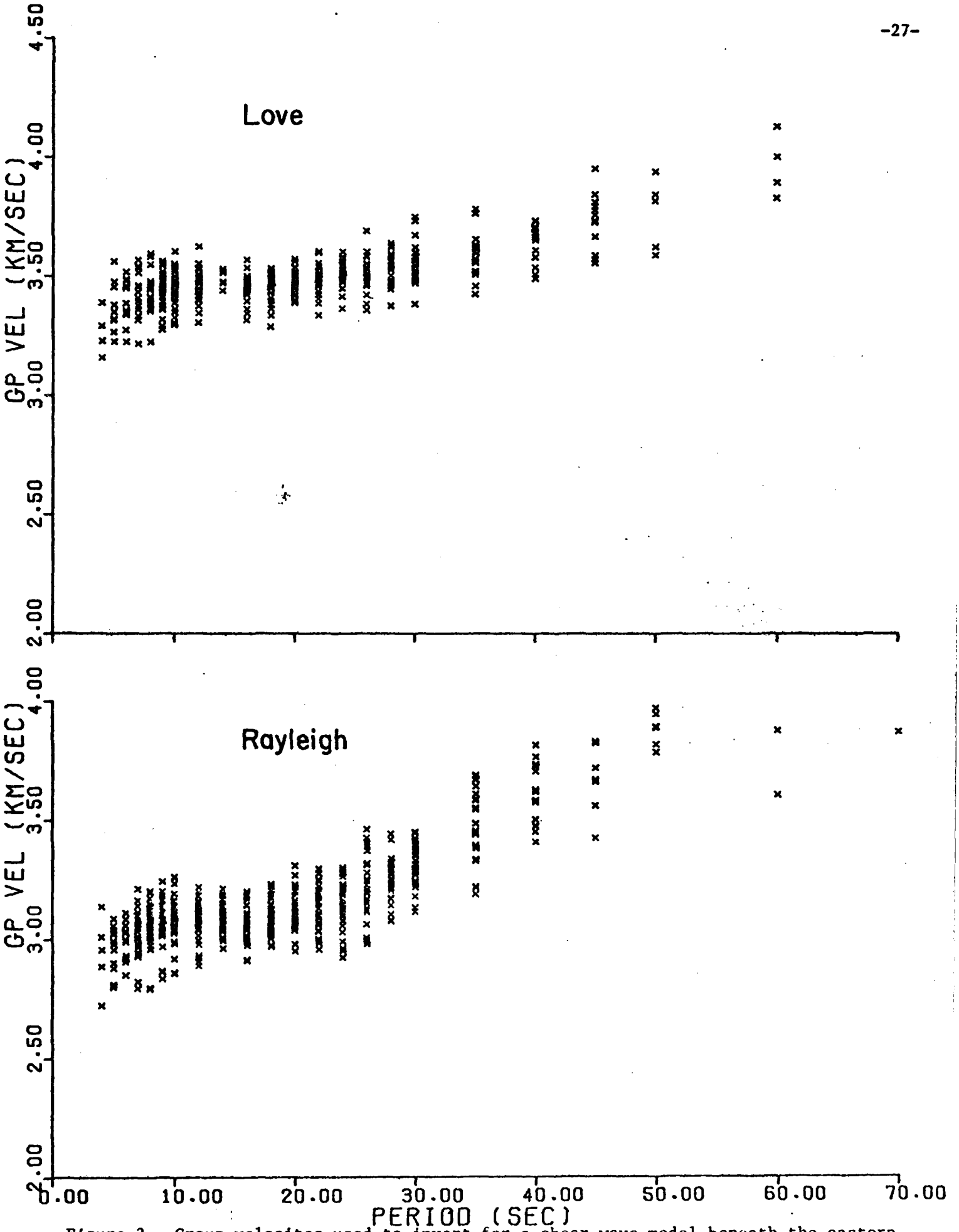

Figure 3. Group velocites used to invert for a shear wave model beneath the eastern United States. These values were obtained after windowing according to amplitude, azimuth, and distance.

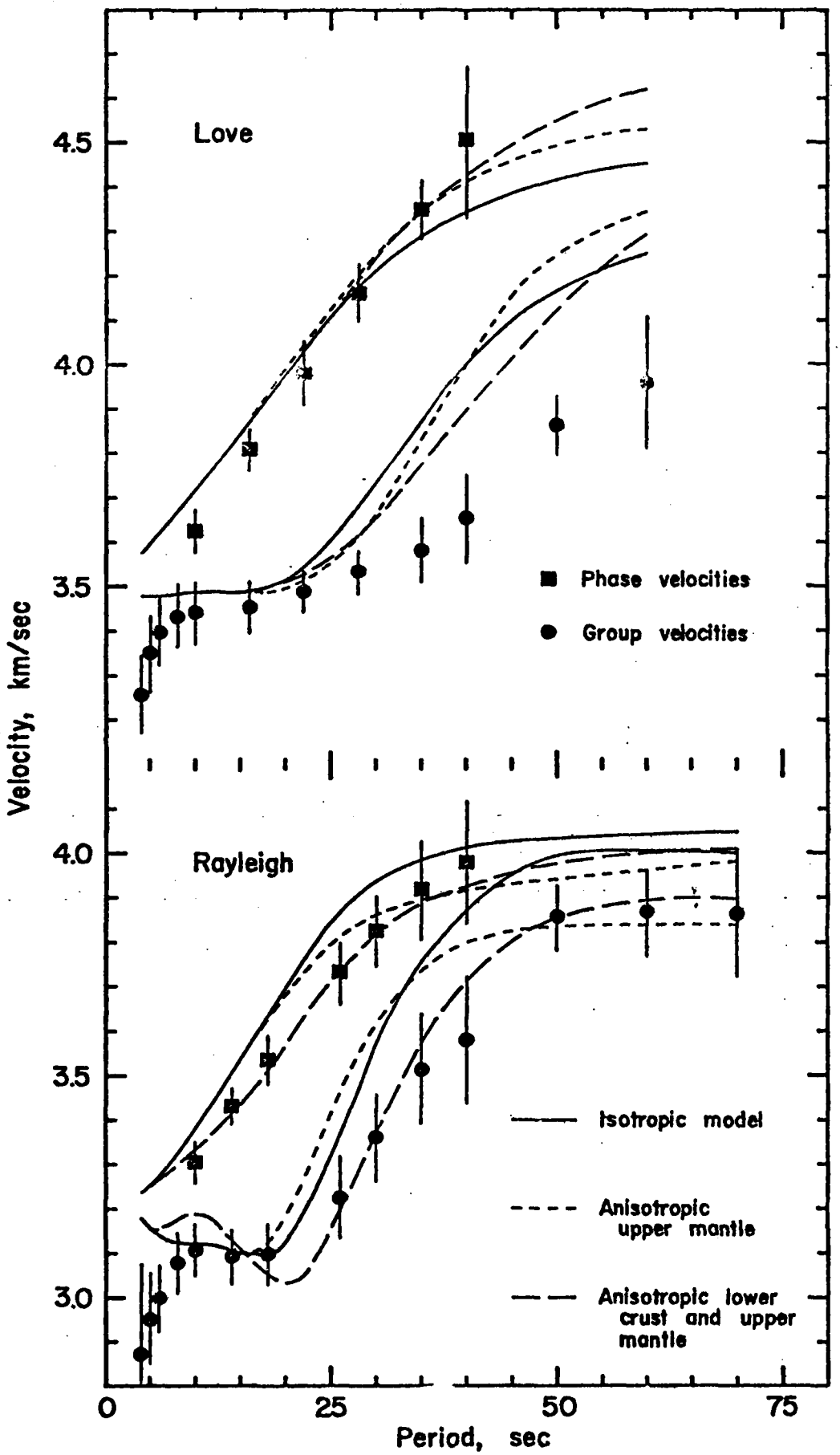

Figure 4. Group and phase velocities for Love and Rayleigh waves across the eastern United States. Vertical bars indicate one standard deviation. These are compared with theoretical values for an isotropic model and two anisotropic models of McEvilly (1964).

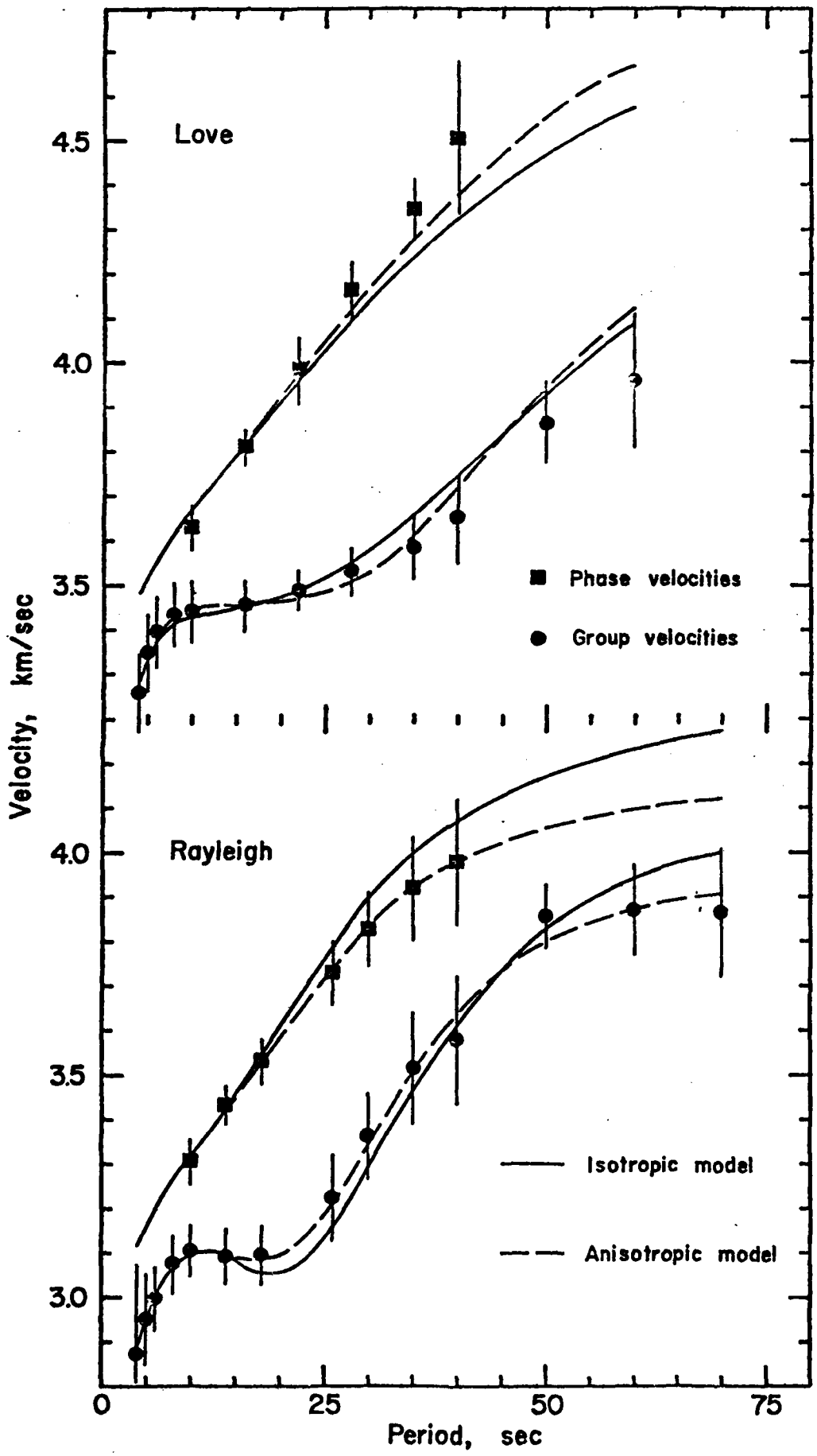

Figure 5. Observed group and phase velocities for the eastern United States. These are compared to theoretical values resulting from the models shown in Figure 6.

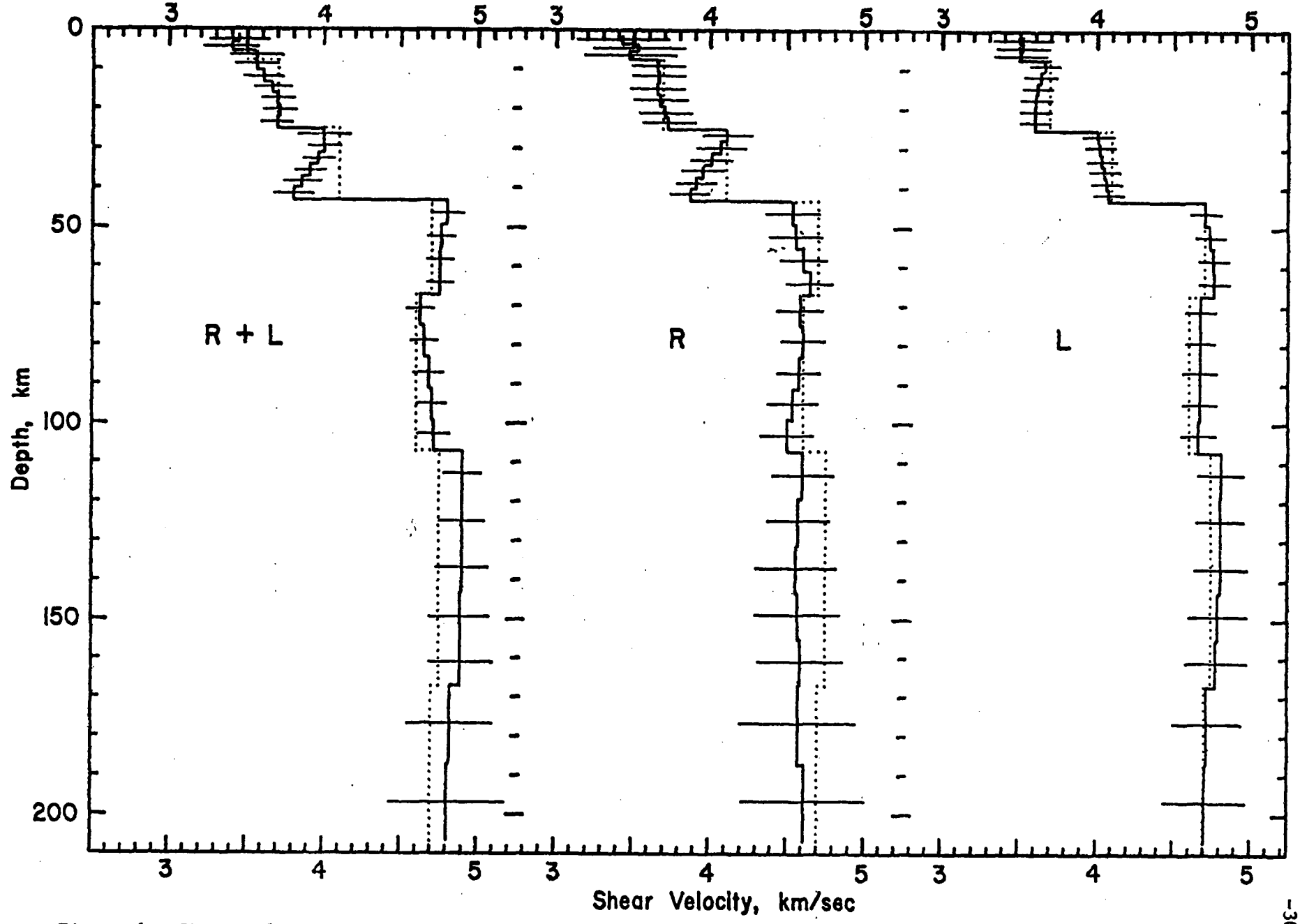

Figure 6. Shear velocity models resulting from the inversion of the group and phase velocities obtained in the present study. Separate inversions were performed for the combined Love and Rayleigh wave data (R+L), the Rayleigh wave data alone (R), and the Love wave data alone (L). The dotted lines

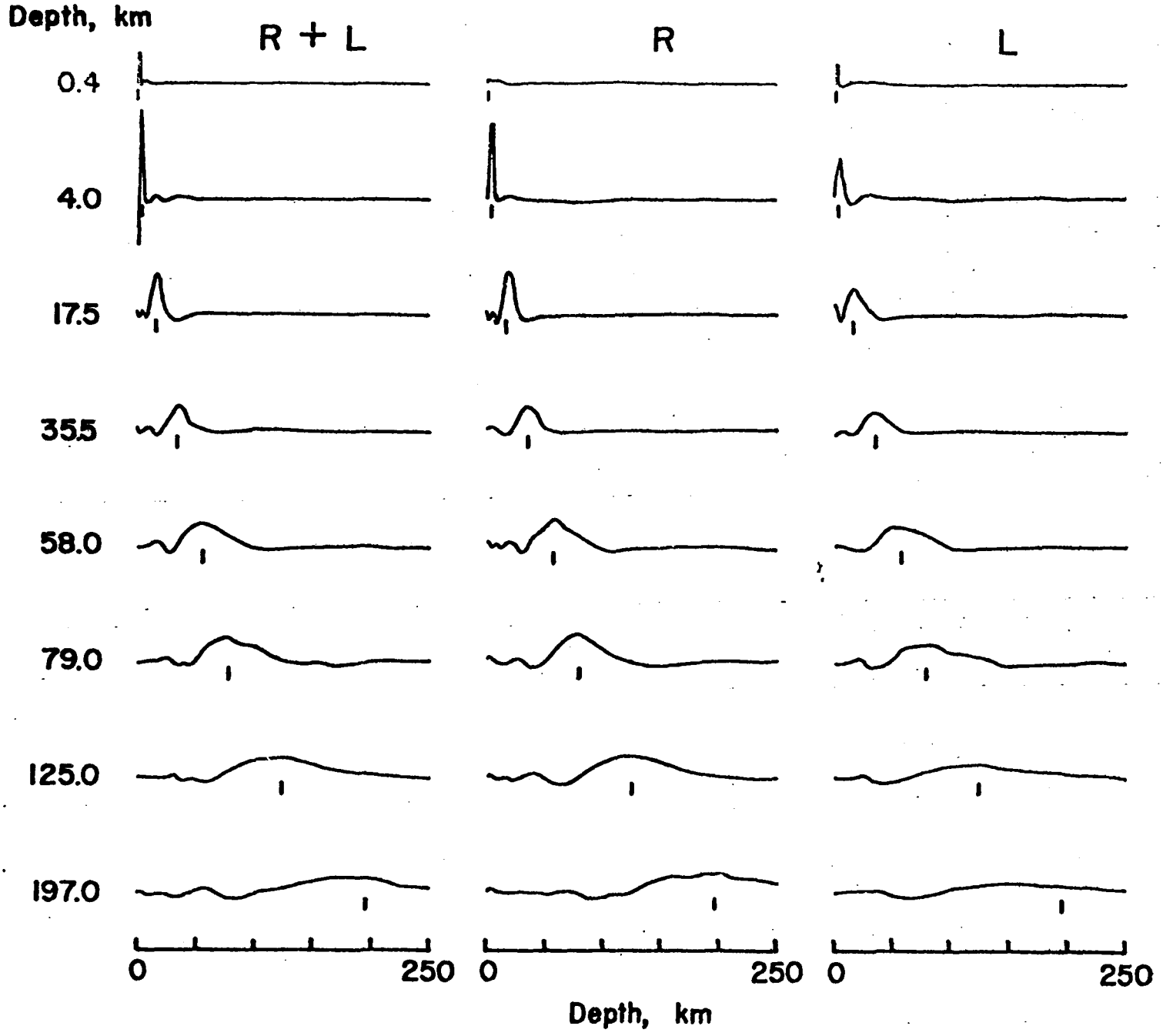

Figure 7. Resolving kernels pertaining the three models of Figure 6.

Q Structures of the Colorado Plateau and the Basin and Range Province from Higher-mode Surface Wave Observations.

by

Chiung-Chuan Cheng

A new method for studying the Q structure along a path between a single earthquake and a single station was presented in the last report. In the past few months, this method has been applied to obtain Q structures of the Colorado Plateau and of the Basin and Range province. One path was used in the study for the Colorado Plateau, and three paths were studied individually for the Basin and Range province. Figure 1 shows these four paths.

Data Collection and Analysis

For each path, the long-period vertical component seismogram was digitized over a time interval which included the entire Rayleigh wave train. These data were then Fourier-transformed. The instrument response was removed and geometrical spreading corrected to a distance of 1000 km. After the application of the multiple filter technique (Dziewonski et al., 1969; Herrmann, 1973), the amplitudes and group velocities for the fundamental mode Rayleigh wave were extracted at periods of interest. Since the group velocities of higher modes overlap among themselves, only the net results of the superposition of higher modes were obtained.

Group velocities of fundamental and higher-mode Rayleigh waves thus obtained have been compared to values computed from P and S wave velocity models given by Keller et al., (1976). Observed group velocities for the Colorado

Plateau path shows a good agreement with their "Northern Colorado Plateau" model, whereas group velocities observed from all three Basin and Range paths are systematically higher than those derived from their "Eastern Basin and Range" model, with differences of not more than 10%. However, both these velocity models have been assumed to be acceptable and used as true values in all theoretical computations in this study.

At each period, every arrival in the filtered signal was identified as either the fundamental mode wave or a higher mode wave if it traveled with a velocity within 10% of the theoretical value, of either the fundamental mode or a higher mode, respectively.

Figures 3(c), 4(c), 5(c), and 6(c) show the observed spectra for each path plotted with amplitudes of identified arrivals.

Q Model Tests

Three Q models have been tested for agreement between the theoretical and observed amplitude spectra. All models assume that values of Q_α are twice those of Q_β at all depths. The models differ from one another only in the upper part, from the surface down to a depth of 18 km, where they have Q_β values of 250, 150, and 50, respectively. At all greater depths, Q_β values are 2000 for all three models (figure 2). The first model is similar to the simplified model obtained for the stable interior of North America obtained by Herrmann and Mitchell (1975).

In computing the theoretical amplitude spectra, fault-plane solutions used were those given by Smith and Sbar (1974). The focal depths of all four events were assigned to be 10 km when computing theoretical spectra shown in figures 3, 4, 5, and 6. These values were determined from comparisons of theoretical spectra originally computed for various focal depths, and were in agreement with the depths favored by Smith and Sbar (1974).

In figure 3, the observed amplitude spectra of the Colorado Plateau path is compared with theoretical spectra computed by using Q model 1 and Q model 2. It is seen that the fall-off of higher mode amplitides with decreasing period is greater for the spectrum derived by using Q model 2 than that by using Q model 1. The observed results are explained better by Q model 2.

Although the three Basin and Range paths were studied individually, figures 4, 5, and 6 show that the comparisons are consistent among themselves. Q model 2 has resulted in fall-off of higher mode amplitudes clearly slower than that observed. On the other hand, Q model 3 has resulted in a fall-off which is too fast.

Discussion

Q model 2 has provided an adequate fit between the observed amplitude spectra and the theoretical spectra for the Colorado Plateau path. A proper Q model to describe the observed amplitude spectra of the Basin and Range paths would be a model having Q values between those of model 2 and model 3.

Based on these results, Q values in the upper crust in the Basin and Range province are lower than those in the Colorado Plateau. Nevertheless, Q models with various values in the upper crust as well as in deeper depths will be tested in further study.

Additional paths will be chosen and analyzed, especially for the Colorado Plateau.

As the velocity model now being used for the Basin and Range province gives a discrepancy between theoretical and observed Rayleigh wave group velocities, knowledge about the effect of velocity model used in applying this method is desired. This will be studied by using various velocity models for the Basin and Range province.

References

Dziewonski, A.M., S. Bloch, and M. Landisman, A technique for the analysis of transient seismic signals, Bull. Seism. Soc. Am., 59, 427-444, 1969.

Herrmann, R.B., Some aspects of band-pass filtering of surface waves, Bull. Seism. Soc. Am., 63, 663-671, 1973.

Herrmann, R.B., and B.J. Mitchell, Statistical analysis and interpretation of surface wave anelastic attenuation data for the stable interior of North America, Bull. Seism. Soc. Am., 65, 1115-1128, 1975.

Keller, G.R., R.B. Smith, L.W. Braile, R. Heaney, and D.H. Shurbet, Upper crustal structure of the eastern Basin and Range, northern Colorado Plateau, and middle Rocky Mountains from Rayleigh-wave dispersion, Bull. Seism. Soc. Am., 66, 869-876, 1976.

Smith, R.B., and M.L. Sbar, Contemporary tectonics and seismicity of the western United States with emphasis on the Intermountain Seismic Belt, Geol. Soc. Am. Bull., 85, 1205-1218, 1974.

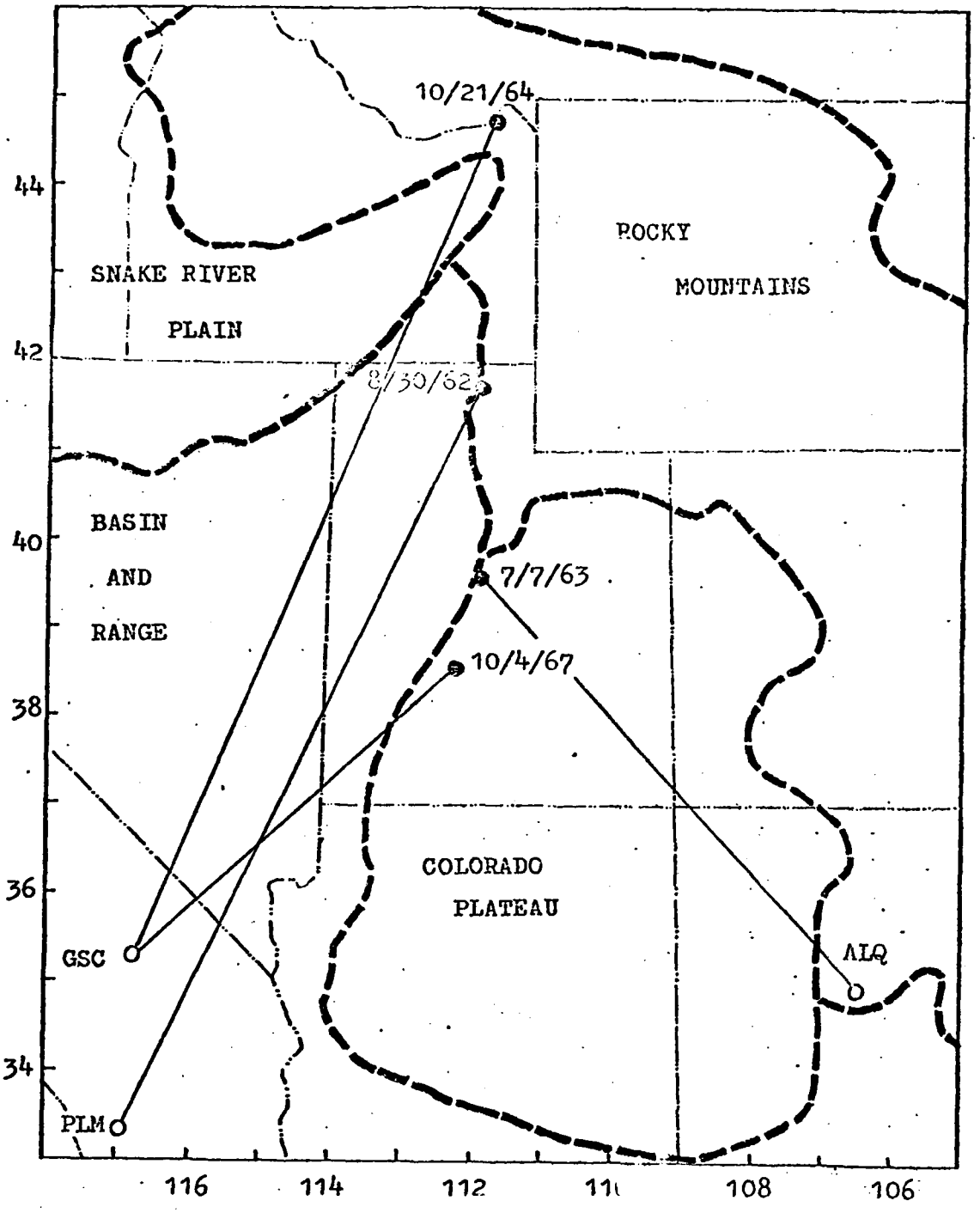

Figure 1. Wave paths analyzed.

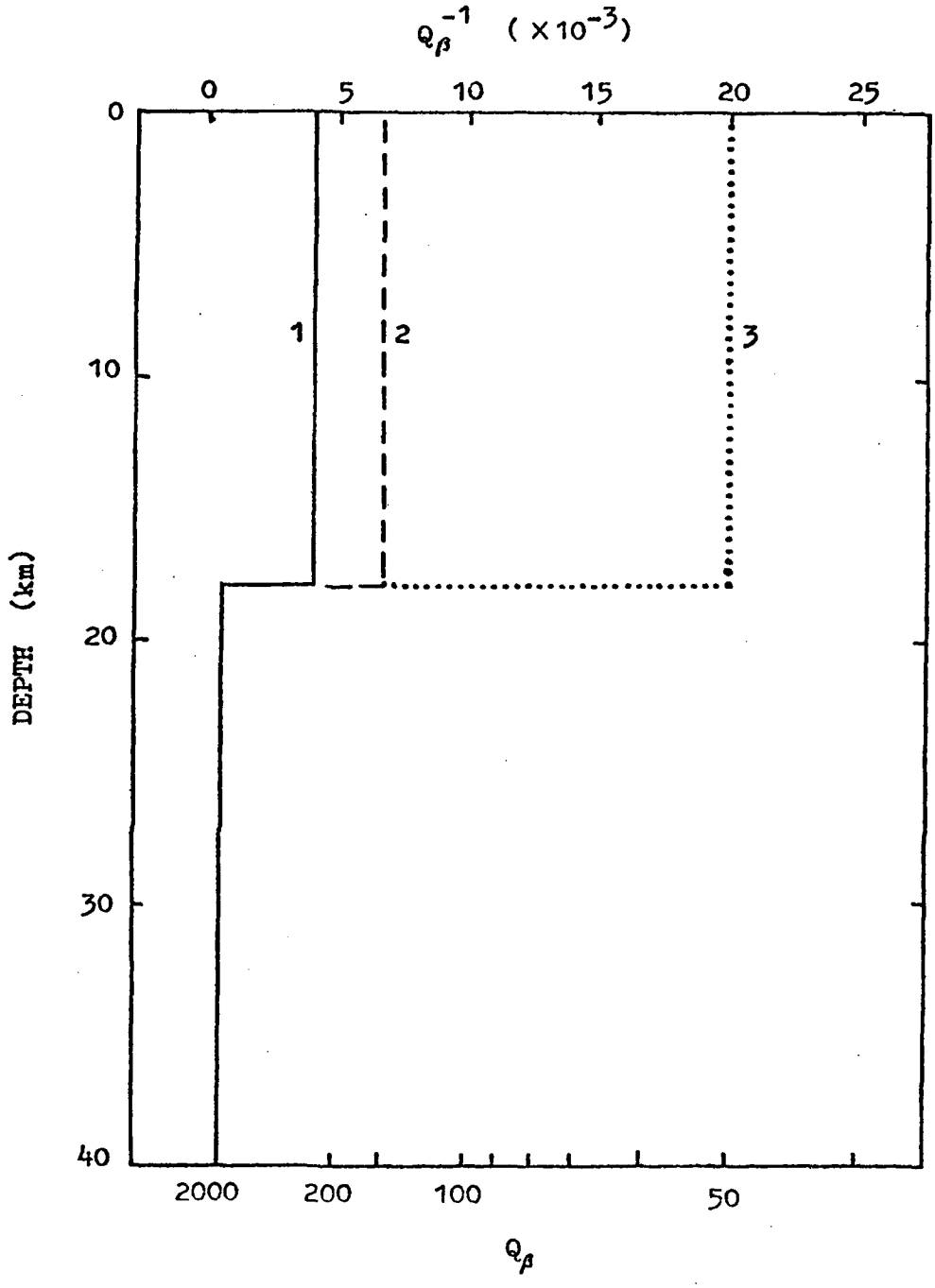

Figure 2. Q models tested.

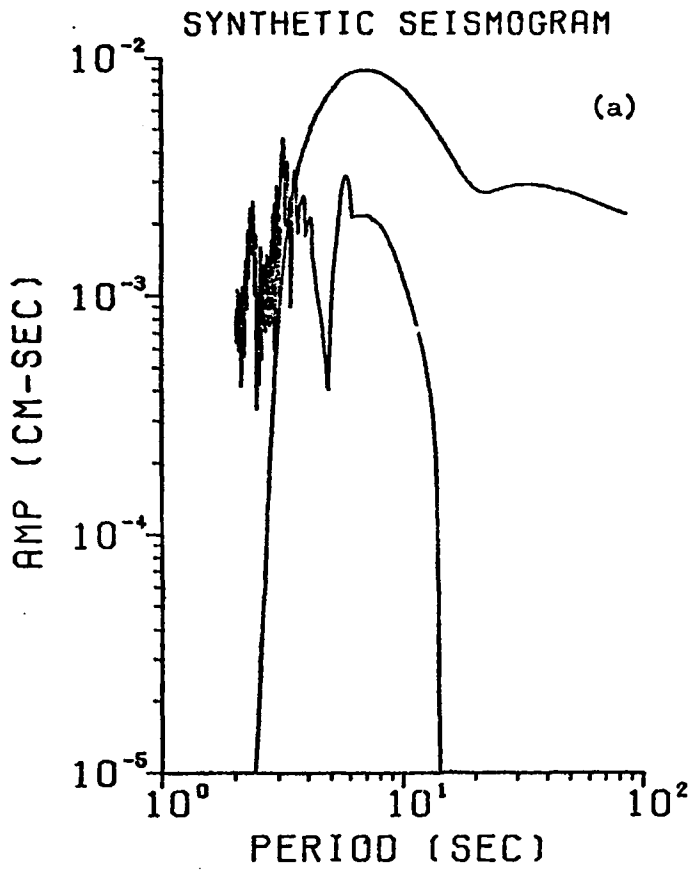

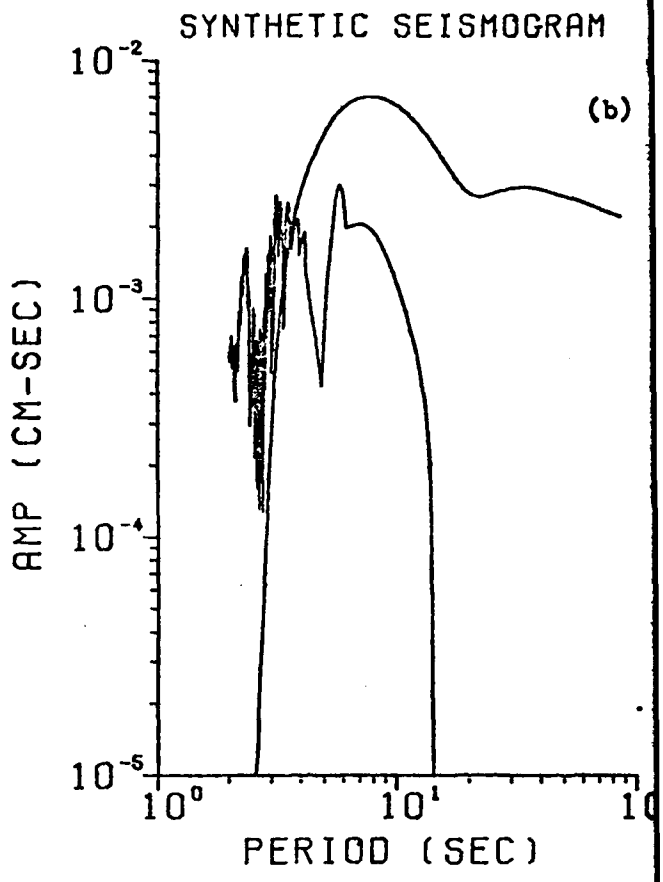

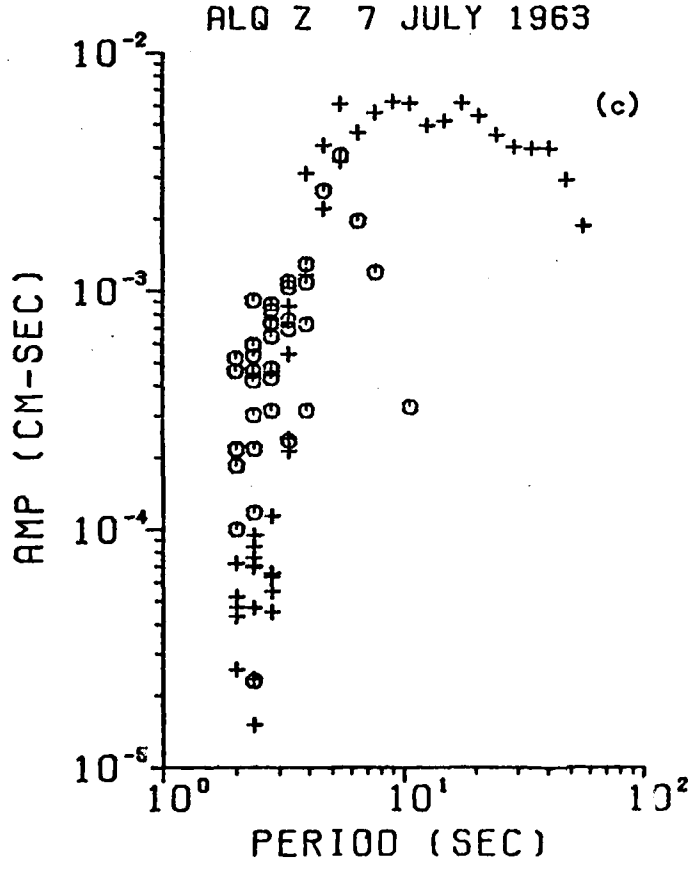

Figure 3. Comparison of theoretical and observed amplitude spectra.

(a) Result for Q model 1.

(b) Result for Q model 2.

(c) Observed fundamental mode (cross) and higher mode (circle) spectra for a Colorado Plateau path.

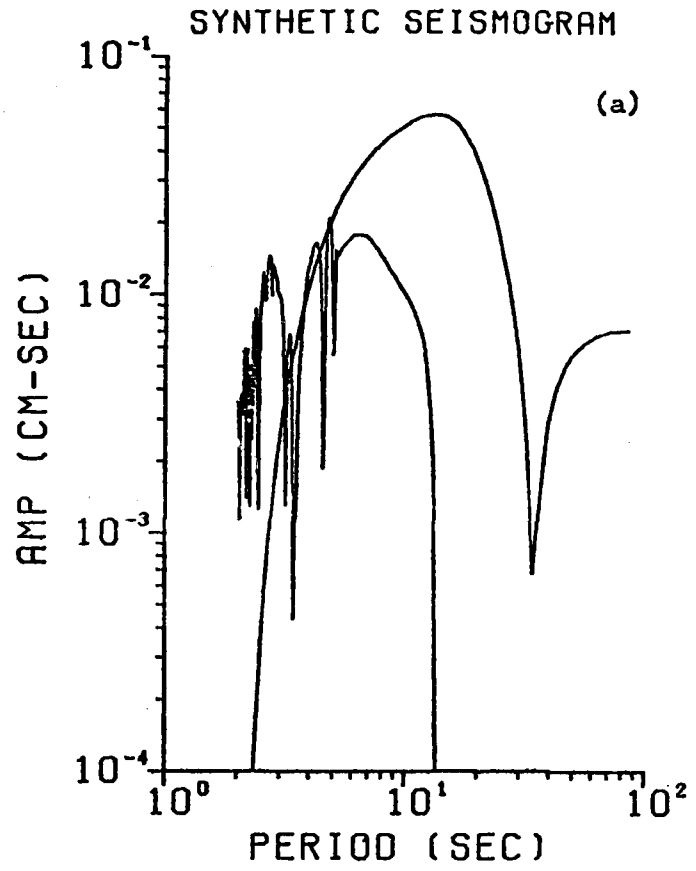

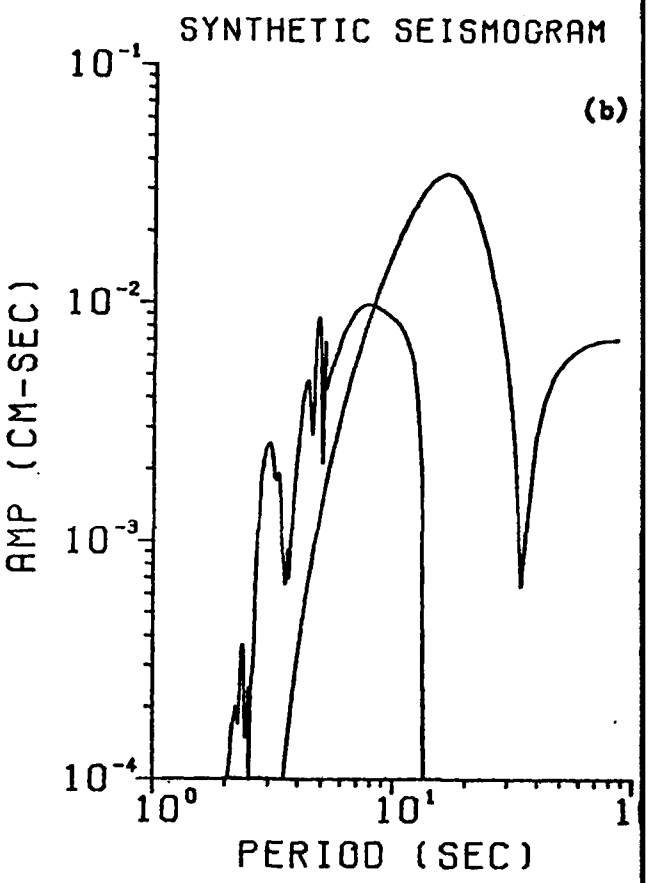

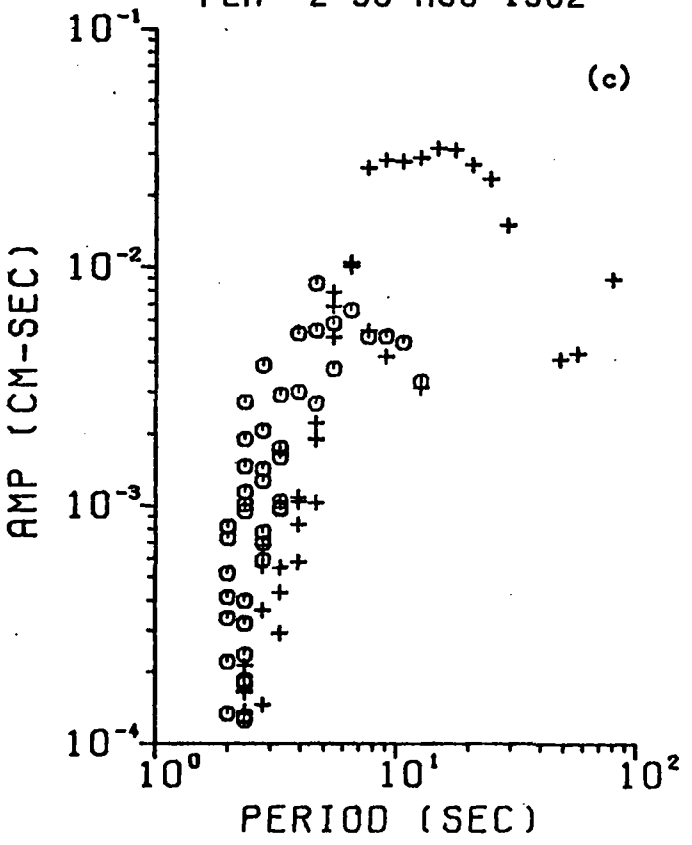

Figure 4. Comparison of theoretical and observed amplitude spectra.

(a) Results for Q model 2.

(b) Results for Q model 3.

(c) Observed fundamental mode (cross) and higher mode (circle) spectra for a Basin-and-Range path.

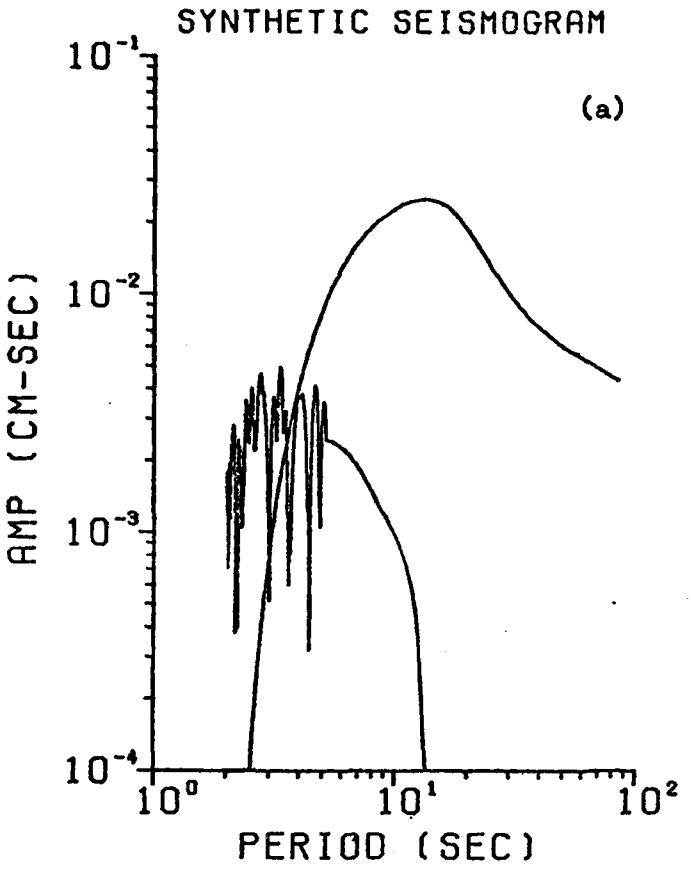

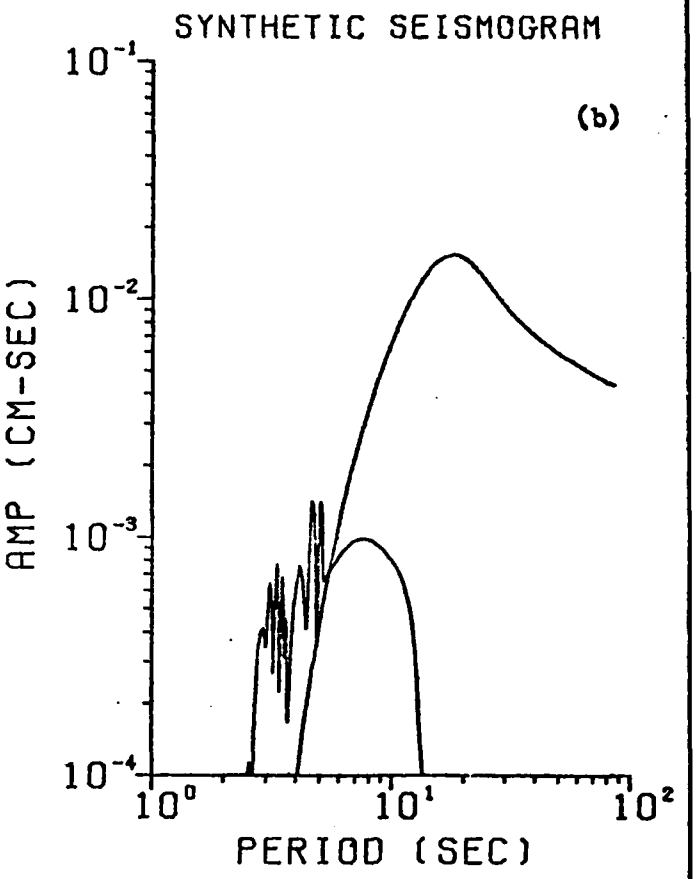

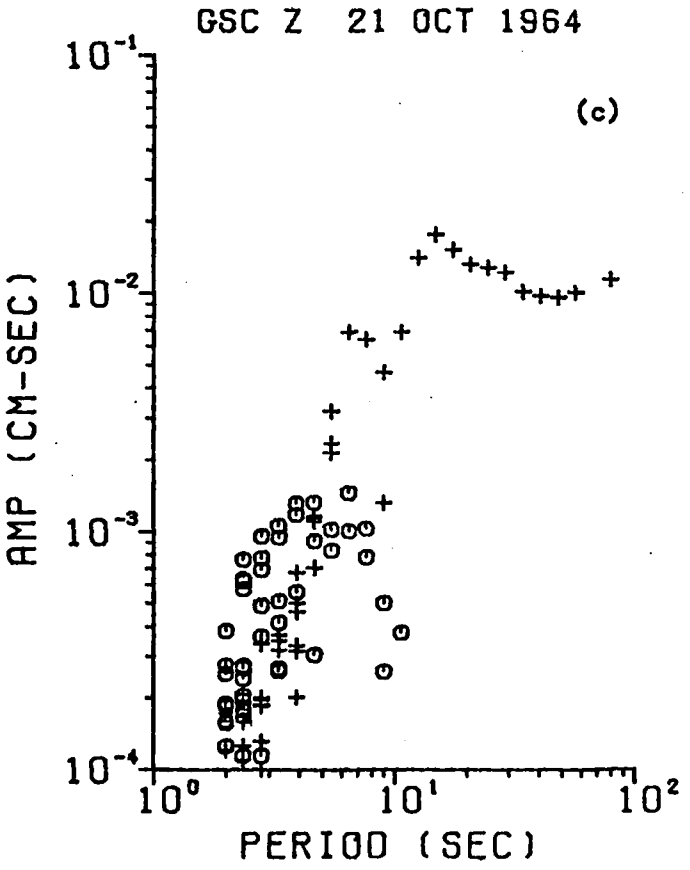

Figure 5. Comparison of theoretical and observed amplitude spectra.

(a) Result for Q model 2.

(b) Result for Q model 3.

(c) Observed fundamental mode (cross) and higher mode (circle) spectra for a Basin-and-Range path.

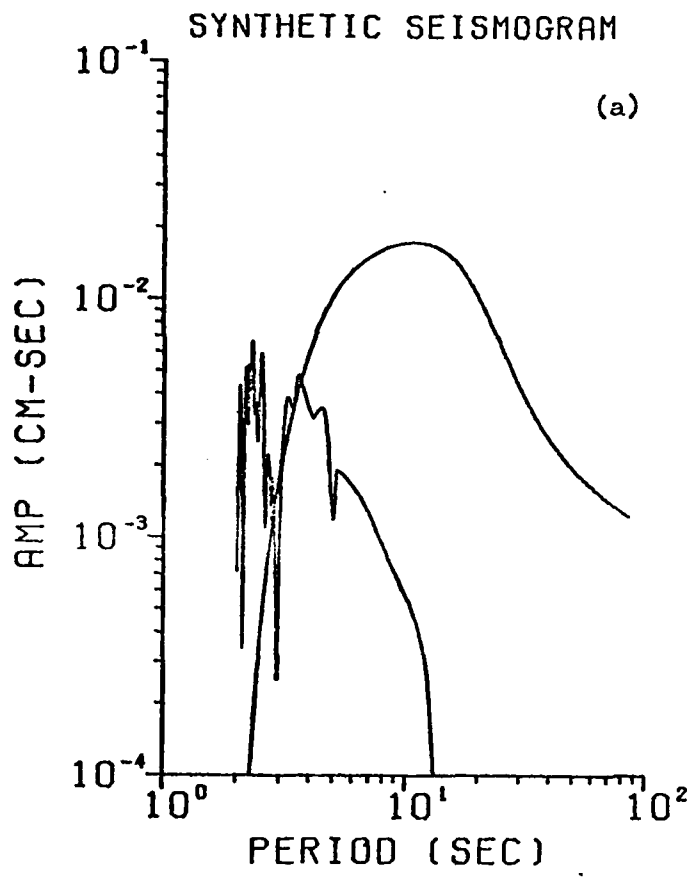

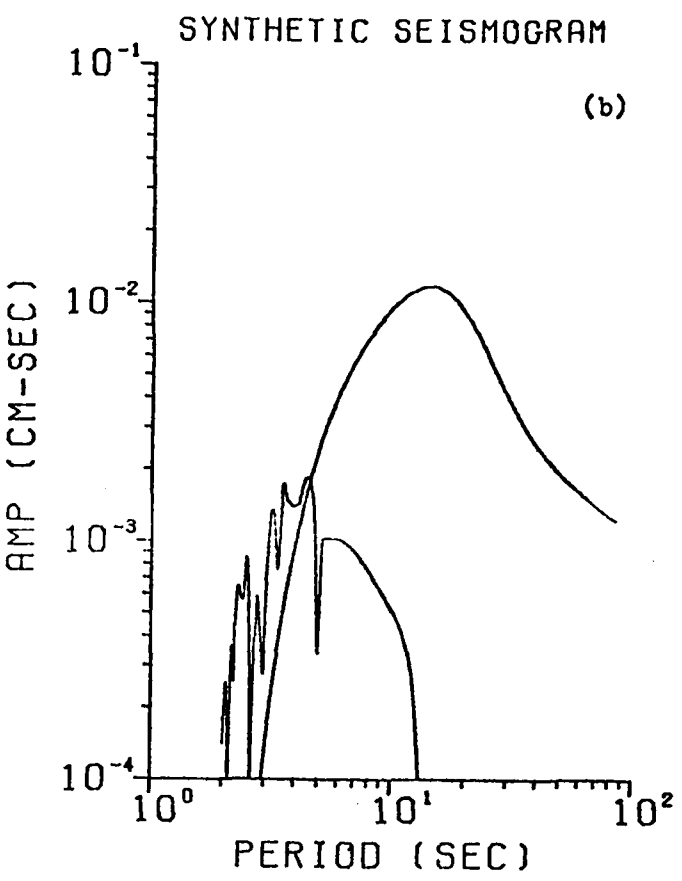

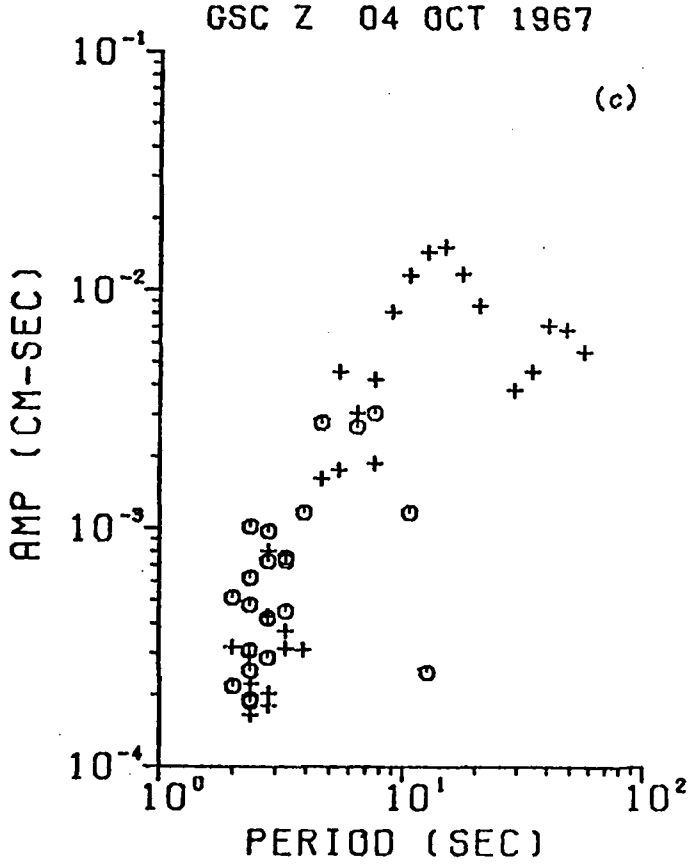

Figure 6. Comparison of theroetical and observed amplitude spectra.

(a) Result for Q model 2.

(b) Result for Q model 3.

(c) Observed fundamental mode (cross) and higher mode (circle) spectra for a Basin-and-Range path.

"On the Existence of a Low-Q Region
Beneath the Southeastern Part of Mexico."

by

Jaime Yamamoto

Introduction

In a previous report (Yamamoto, 1977) the existence of a highly attenuating region located somewhere beneath the southeastern part of Mexico was suggested from the anomalously small P-wave amplitudes observed at a certain range of distance and azimuth. In the present report a more detailed analysis of the data is made in an attempt to reach more definitive conclusion on that matter.

Analysis of Data

The largest foreshock (OT=11:22, h=45 km, Ms=6.3) and aftershock (OT=08:32, h=16 km, Ms=6.4) associated with an earthquake sequence started on April 29, 1970 near the coast of Chiapas, Mexico (14.5 N, 92.8W) are used in the discussion.

Figure 1 is a plot of the observed P-wave amplitude (zero to peak) in cm as measured on the long-period vertical component versus the amplitude measured on the synthetic seismogram computed using a Haskell-Thomson method. From this figure it is evident that amplitudes observed at the eastern United States stations depart considerably from the expected amplitudes assuming a double couple point source and a ratio T/Q = 1 (value that in general is a good approximation to simulate the non-elastic attenuation along the ray-path, see Langston and Helmberger, 1975). One way to reconcile these observations with the theory is by assuming T/Q = 3 or 4 as shown in the figure (solid circles). In this case synthetics were computed using a point source with the appropriate geometry

strike = 292°, Dip = 19°, slip = 72°) located at a depth of 10 km inside a layered medium. The seismic moment (M_o) was assumed to be 10^{26} dyne-cm and the source function was represented with a trapezoid of unit area defined with three time segments (2.5, 1.0, 2.5 seconds).

The same pattern is seen in the foreshock as shown in Figure 2. In that figure values of 50 km for the source depth and 6 x 10^{25} dyne-cm for M_o and a ratio T/Q = 1 were assumed. All the other parameters were taken to be the same as in the case of the aftershock.

In the previous report it was pointed out that foreshock shows a secondary arrival approximately 8 seconds after the first arrival and that this secondary onset (supposedly due to a multiple source) disappears for a narrow interval of distance and azimuth. Figure 3 is a polar plot centered at the epicentral region and shows with solid circles stations at which a clear secondary arrival was recorded. Open circles denote stations at which no secondary arrivals are observed. Semi-solid circles and encircled plus signs, stations with no clear secondary onset and unreadable seismograms respectively. Examples of observed seismograms are shown in the figure. Notice that the apparent period of the P-wave recorded at WES is appreciably longer that the one at BKS even though both stations have similar epicentral distance suggesting that the ray-path corresponding to station WES has a higher value of T/Q as compared with BKS. The disappearance of the secondary arrival is unlikely to be due a simple geometrical effect since some European stations (ESK for example) show it. In addition, their P-wave amplitudes agree reasonably well with the theory. Notice that WES and ESK have practically the same azimuth.

P-wave form analysis also seem to lead to the same conclusion. Figure 4 shows the observed and synthetic seismograms. Two identical source functions as described previously separated by 8 seconds were used. Most of the modelled

stations are consistent with the value T/Q = 1 except the eastern U.S. stations (see AAM and WES) for which T/Q = 4 is necessary to match synthesized and observed signals. The agreement between synthetics and observed seismograms is remarkably good taking into account that all the synthetics in Figure 4 were computed with the same source function.

Discussion and Tentative Conclusion

From the analysis of the previous figures, it seems that the signals recorded at eastern United States stations for these particular events have crossed a region of high attenuation. This region, if it exists, may be located beneath the recording stations, near the source or in between.

Independent studies by Mitchell (1973) and Nuttli (1973) however, indicate that eastern U.S. is characterized by a low attenuation as compared with the west. Molnar and Oliver (1969) on the other hand, have concluded that the Gulf of Mexico is a very stable region as transmission of shear waves is concerned.

Therefore, these results seem to indicate that the anomalous region, if any, is likely to be located near the source and its Q-value is more than 4 times lower than the Q-value associated with the surrounding asthenosphere. In Figure 5 a possible configuration for this zone is shown. Its shape, dimensions and position are, however, highly conjectural.

An alternative explanation of the available data is that the abnormal P-wave amplitude distribution is due to a defocusing effect produced by refractions in a laterally heterogeneous upper mantle near the source. Molnar and Oliver (1969) however, found that some paths traversing active volcanic belts of Mexico (which is our case) and Central America show attenuation of Sn waves (see their Figure 9). Molnar and Sykes (1969) observed when locating earthquakes in Mexico and Central America, that stations located northeast from

the epicenter at large distances show early arrivals. Conversely, arrivals at near stations were delayed. These two results seem to support our conclusion. However, further work is planned to determine whether a defocussing effect can be ruled out as a cause for the low amplitudes. One approach will be to analyze S arrivals. If a T/Q value of 4 is required for P waves, then the S waves should show an extremely great attenuation if they pass through the same region.

REFERENCES

Langston, C.A. and D.V. Helmberger, "A Procedure for Modelling Shallow Dislocation Sources", Geophys. J. Roy. Astron. Soc., 42, 117-130, 1975.

Mitchell, B.J., "Surface Wave Attenuation and Crustal Anelasticity in Central North America", Bull. Seism. Soc. Am., 63, 1057-1071, 1973.

Molnar, P. and J. Oliver, "Lateral Variations of Attenuation in the Upper Mantle and Discontinuities in the Lithosphere", J. Geophys. Res., 74, 2648-2682, 1969.

Molnar, P. and L.R. Sykes, "Tectonics of the Caribbean and Middle America Regions from Focal Mechanisms and Seismicity", Geol. Soc. America, 80, 1639-1684, 1969.

Nuttli, O.W., "Seismic Wave Attenuation and Magnitude relations for eastern North America", J. Geophys. Res., 78, 876-885, 1973.

Seely, D.R., P.R. Vail and G.G. Walton, "Trench Slope Model", in: The Geology of Continental Margins, Springer-Verlag, New York, 249-260, 1974.

Yamamoto, J., Research in Seismology. Semi-Annual Technical Report. 1 April to 1 September 1977. ARPA Contract Number F44620-73-C-0042. Saint Louis Univ., pp. 55-66, 1977.

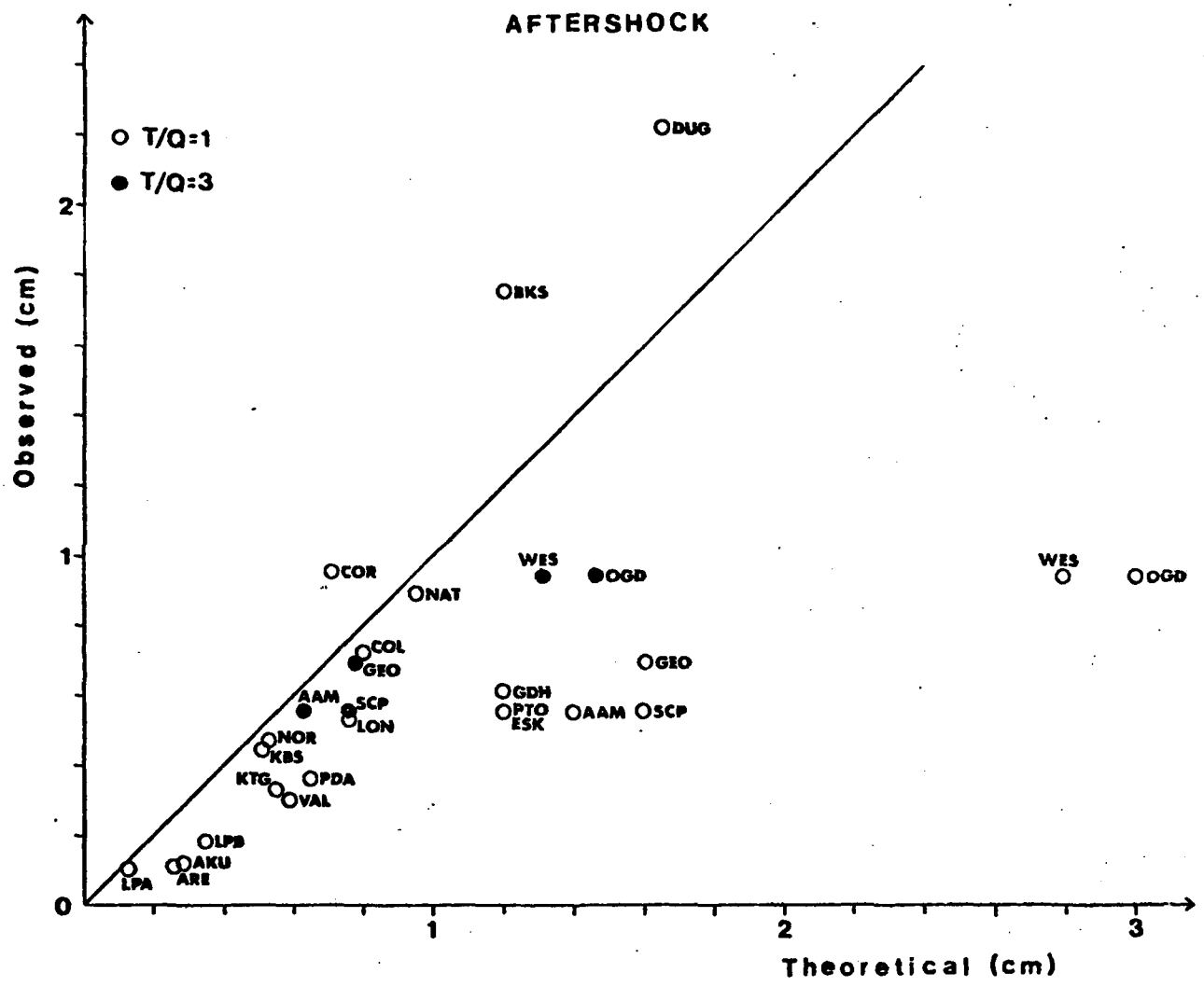

Figure 1. Comparison of observed and theoretical amplitudes for the aftershock.

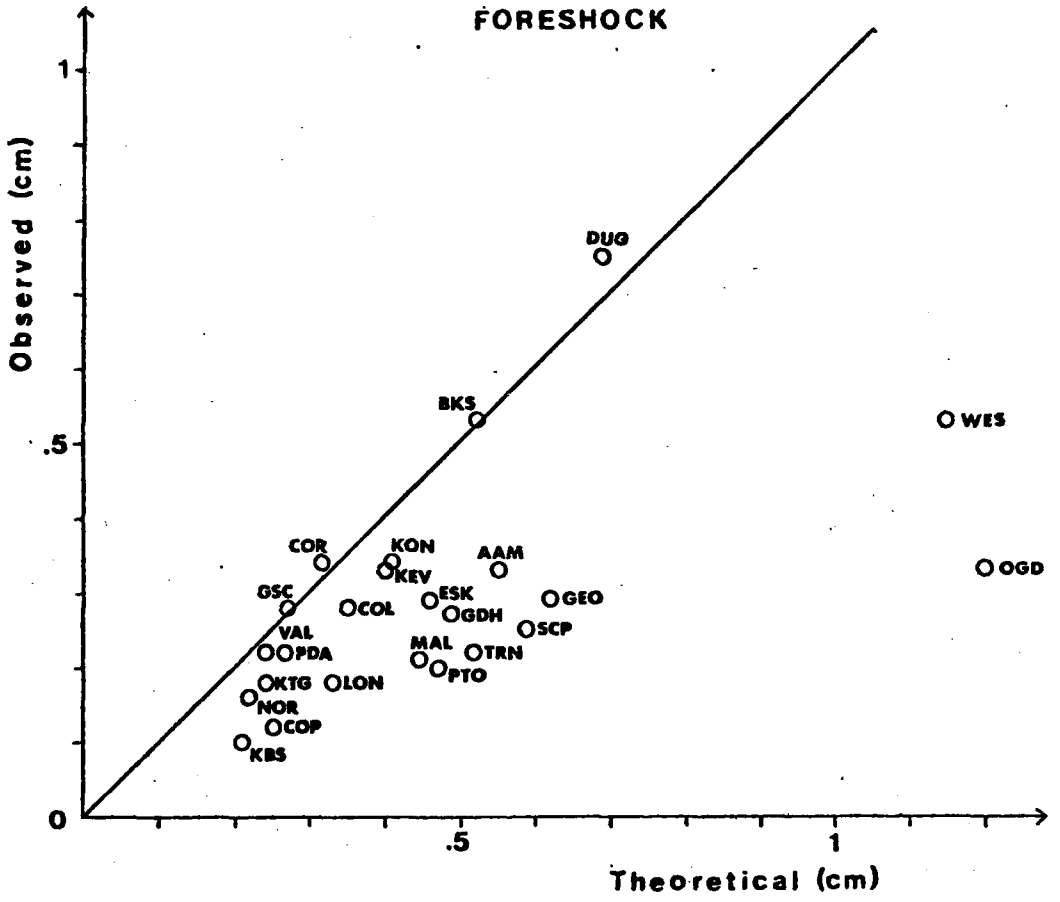

Figure 2. Comparison of observed and theoretical amplitudes for the foreshock.

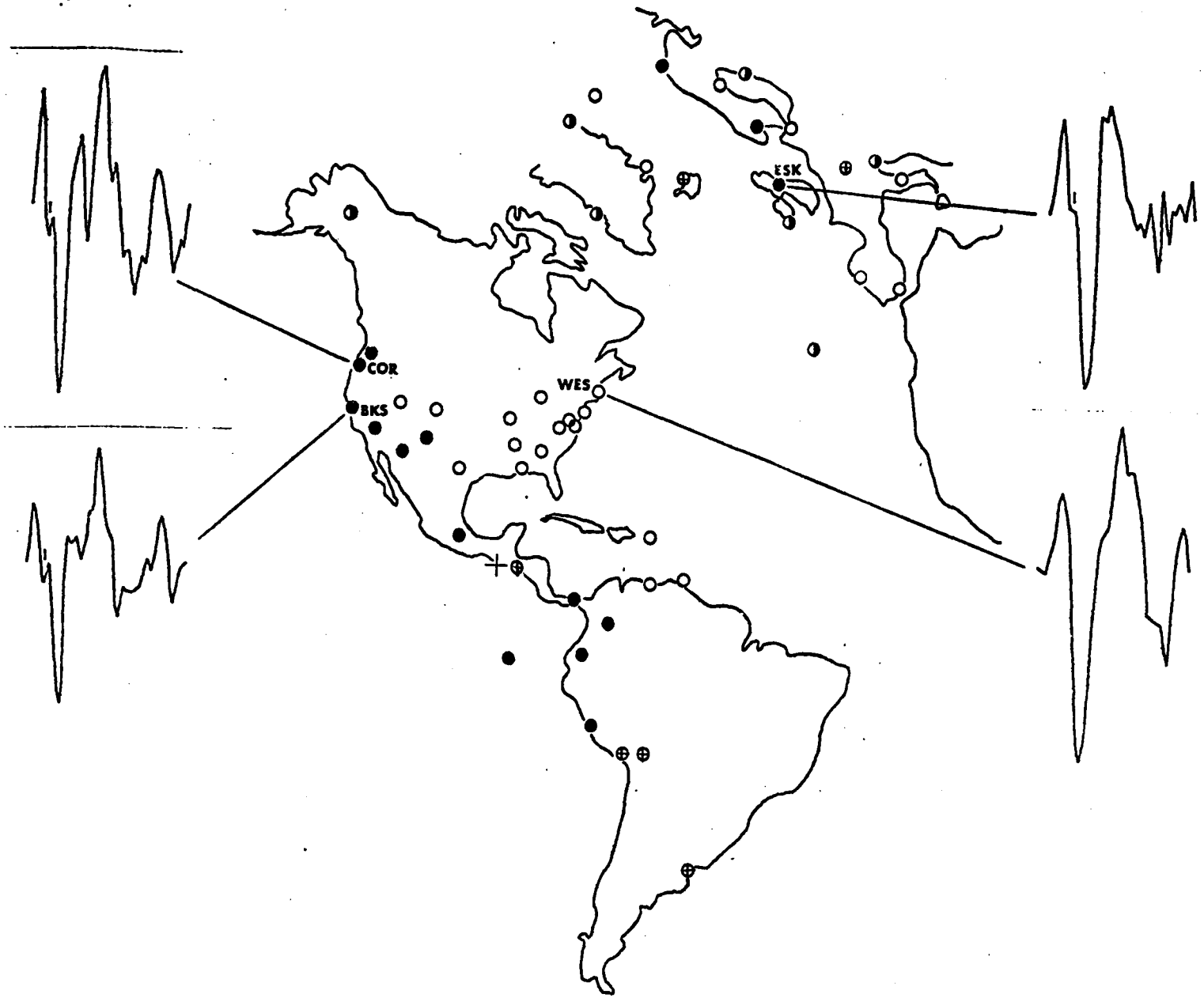

Figure 3. Illustration of attenuated multiple at station WES.

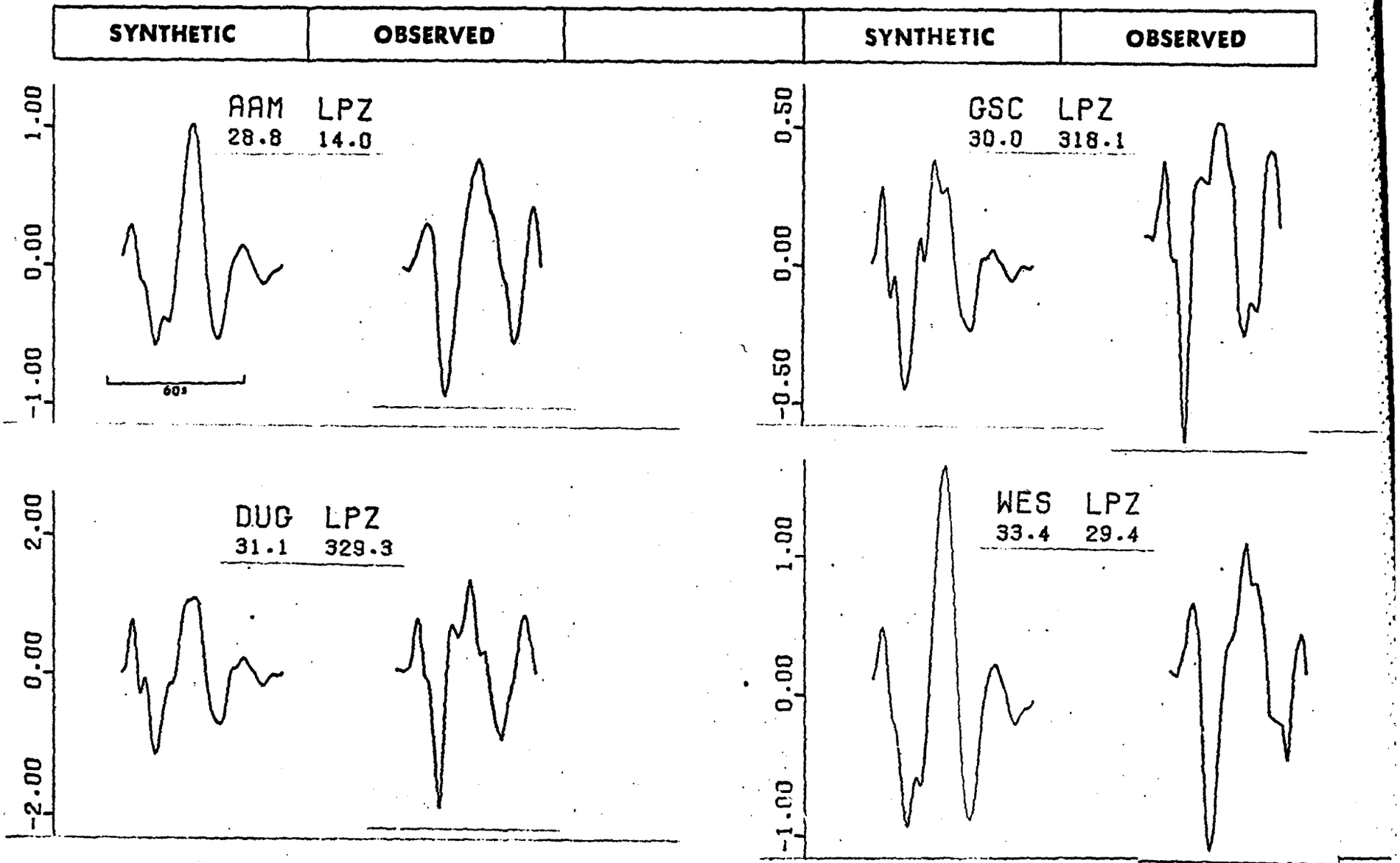

Figure 4. Synthetic and observed seismograms.
Vertical scale in cm. The number below the station code
is the distance in degrees and the one below the component identification is the azimuth.

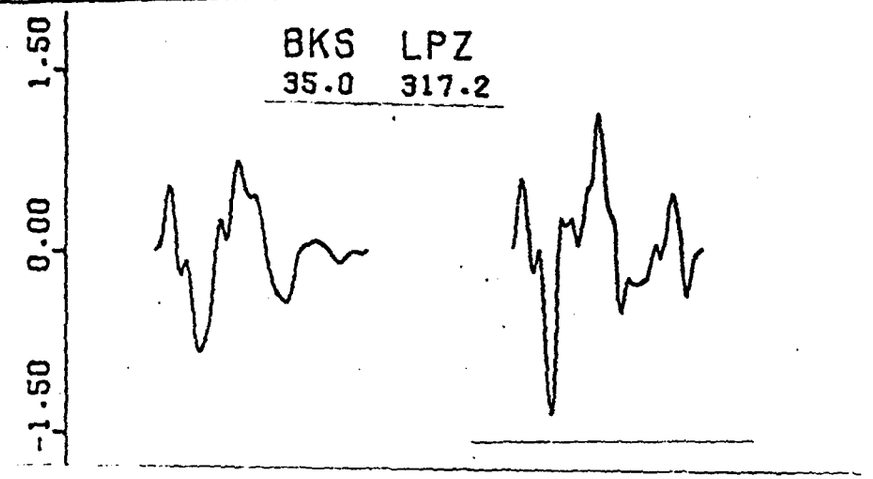

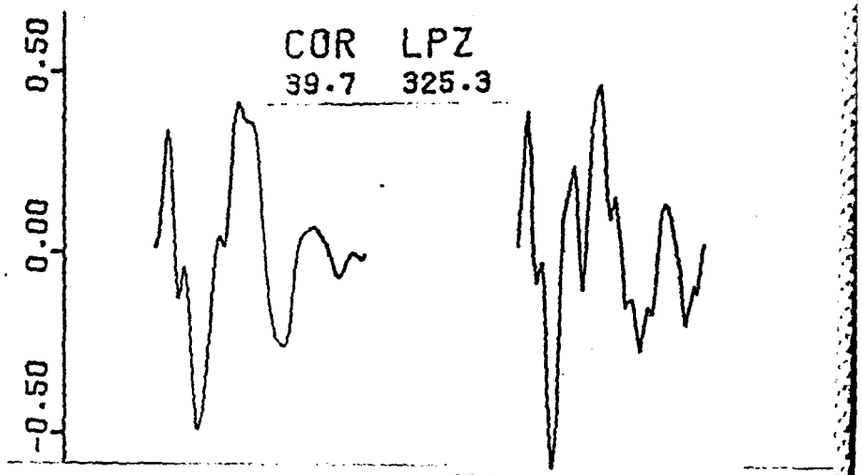

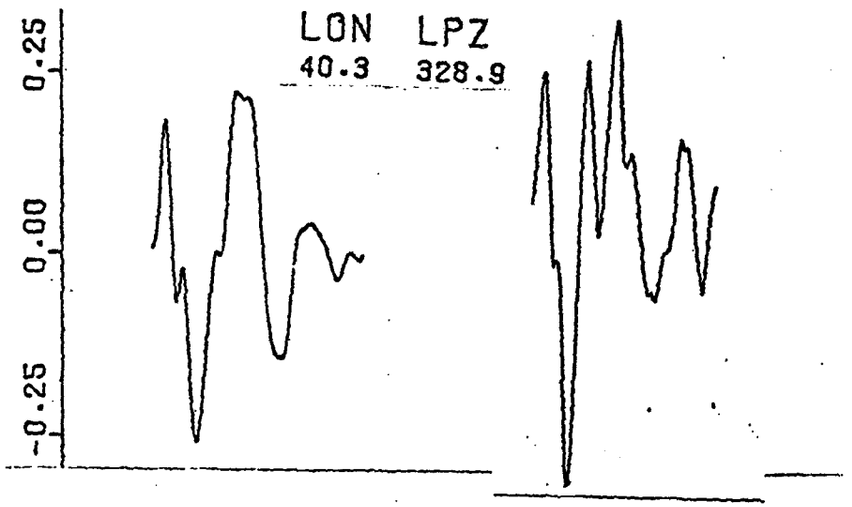

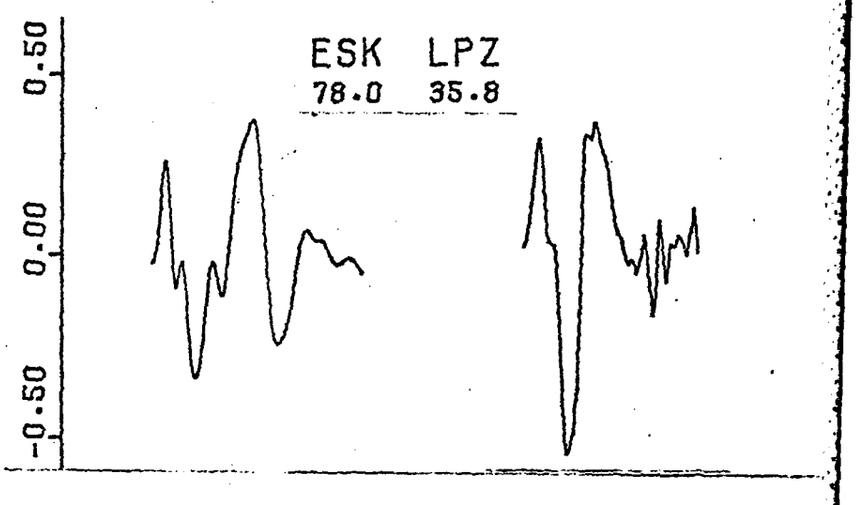

Figure 4 (cont'd).

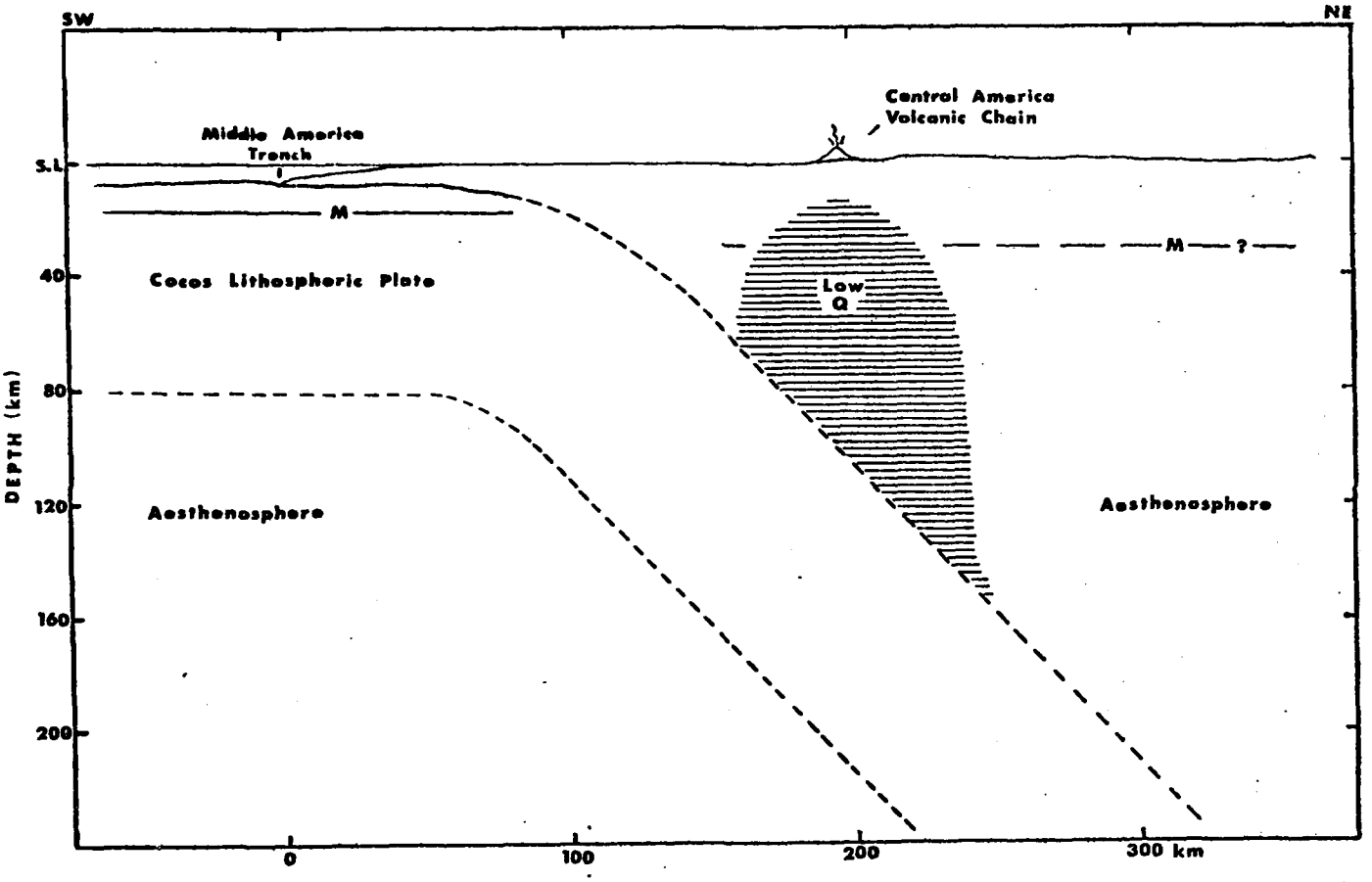

Figure 5. Position of the low-Q region as inferred from the analysis. Structural model including descending slab boundaries taken from Seely et al. (1974).

P-WAVE SPECTRA OF EARTHQUAKES

by: Huei-Yuin (Wen) Wang

Many authors have studied the scaling law of earthquakes. The scaling law, by using the assumption of similarity, is the concept of relating earthquakes of different sizes by a single seismic source parameter model. Aki (1967, 1972) derived his ω-square model by assuming all earthquakes produce a constant stess drop independent of source size. For this model, the corner frequency is inversely proportional to the fault length and the seismic moment is proportional to the cube of the fault length. Further testing of the ω^2-law Aki (1972), confirmed that it is valid only for large earthquakes ($M_S > 6$) and for periods larger than 10 sec. The scaling relations may be more complicated for small earthquakes. The stress drop of these earthquakes is in the range of 10 to 100 bars.

Later on, Chouet et al (1978) used the coda method to scale for small earthquakes, for periods shorter than 10 sec. They found that the stress drop increases with magnitude for small earthquakes.

Geller (1976) presented source spectra for P waves, based on a data set of 41 earthquakes. He found that if effective stress and static stress drop are equal and the fault length and width are related by L = 2W, the length can be used as the sole free parameter in a Haskell model to derive a scaling law for P-wave and surface-wave spectra.

P-wave spectra have been used to scale eight large and shallow Eurasian earthquakes. Those spectra are all corrected for instrument response, anelastic attenuation, geometrical spreading, radiation pattern, and equalized to a distance of 30°, before obtaining the seismic moment M_o.

The Hanning window, which is

$$W(t) = \begin{cases} 0.5\left(1 + \cos\frac{\pi t}{T_{max}}\right) & 0 \leq |t| \leq T_{max} \\ 0 & |t| > T_{max} \end{cases}$$

where t = transient time, T_{max} = digitized length of record is employed for smoothing of the observed amplitude spectra of P-wave, so that the spectrum contains most of the energy in the central lobe and an insignificant portion in the side-lobes.

Data from WWSSN records have been studied. Table 1 is the list of earthquakes studied. Most long-period records of earthquakes 6, 7, and 8 are off-scale. Thus it is not generally possible to obtain reliable m_b and M_s values. As such, ISC values for m_b and NEIS values for M_s are used as the average values.

The seismic moment is determined from the long-period level of the surface-wave or body-wave amplitude spectrum. Since long-period waves are less affected by structural complexities than the short period waves used for the determination of earthquake magnitude, the seismic moment can be considered as one of the most reliably determined instrumental earthquake source parameters. For large earthquakes, the value of M_o determined by different investigators seldom differs by a factor of more than two (Kanamori and Anderson, 1975).

The seismic moment (M_o), stress drop ($\Delta\sigma$), source dimension (r_o), and corner periods (T_{01}, T_{12}, T_{02}) shown in Table 2 are calculated on the basis of Brune's model (1970). The equations are:

$$M_o(P) = \frac{\Omega_o(P)}{R\theta\phi(P)}\, 4\,\pi\,\rho R\alpha^3$$

$$r_o(P) = \frac{2.34\,\alpha\,T_{01}(P)}{2\,\pi}$$

$$\Delta\sigma(M_o, r) = \frac{7}{16}\,\frac{M_o}{r_o^3}$$

Inappropriate values of $R\theta\phi$ (radiation pattern) can cause significant errors in the determination of M_o. Especially, when the station is near the node of P-wave spectral amplitude, its moment is overestimated by underestimating $R\theta\phi$. Accordingly, we only accept a moment determination when $R\theta\phi$ is larger than 0.05 (Nuttli and Gudaitis (1966), Hanks and Wyss (1972)). The best fault plane solution is obtained by testing the P-wave spectra from all stations for the event, and minimizing the difference between those spectral levels after they are corrected for $R\theta\phi$.

From m_b-Ms values or m_b-M_o(P) values, two events could be considered to be anomalous earthquakes, earthquake 1 and earthquake 6. The m_b value of earthquake 1 is about 0.3 units larger, while its corner period (T_{01}) and source dimension (r_o) are about the same as those for the other non-anomalous earthquakes.

For earthquake 1, only four observations (COL, NUR, QUE, SHI) of the available records have been studied. The average values are 5.91 and 5.63, respectively, for m_b and M_S. By the m_b:M_S criterion, this event could be considered to be non-anomalous.

The m_b value of earthquake 6 determined by us is about 1.0 unit larger than the value calculated by ISC. Our value is based on eleven observations with standard deviation of 0.32 units. We prefer to use our m_b value for earthquake 6. From Table 2, it also tells us that this event has anomalous characteristics, with a smaller corner period (6.67 sec) and source dimension (17.15 km).

The P-wave spectra are characterized by three straight lines and two corner periods (T_{01}, T_{12}). The shapes are similar to the idealized spectra derived from Geller (1976) in that they show a gradual transition from T^o to T^3 asymptotes.

The estimated values of $\Delta\sigma$ in Table 2 seem to be low either for large earthquakes ($M_S \geq 6$) or small earthquakes. This may result from an overestimation of r_o, because $\Delta\sigma$ varies as r_o^{-3}.

If an earthquake results in the complete release of the effective stress at the time of occurrence, the effective stress must be equal to the stress drop (Brune, 1970). Trifunac (1972) demonstrated that the effective stress is, on the average, about constant for large earthquakes. Kanamori and Anderson (1975) found that stress drops are 10 to 30 bars for most interplate earthquakes and 30 to 100 bars for most intraplate earthquakes. An apparent stress which is about half the stress drop is accepted. Chinnery (1964) and Aki (1972b) calculated that the stress drop in shallow earthquakes is 10 to 100 bars. But for smaller earthquakes, the stress drop ranges from 0.5 to 300 bars (Wyss and Brune, 1968).

Figure 1 shows the relation between log M_o and M_S. The solid lines of constant apparent stress are taken from Kanamori and Anderson (1975) with slope of 3/2. The dashed lines are from Geller (1976). The conclusion that larger magnitudes correspond to larger apparent stresses is valid for all the events. Earthquakes 7 and 8, whose Ms values are 7.6 and 7.9, have stresses of more than 100 bars. This observation is not in agreement with Aki's model. Earthquake 7 is an Aleutian earthquake. Considering the focal mechanism for this earthquake, one of the planes is nearly horizontal, dipping to the northwest, whereas the other plane is nearly vertical. The fault motion is an underthrusting if the horizontal plane is taken as the fault plane (Stauder, 1968). Aki (1972) also found that the ω-square model fails for two earthquake pairs in the Aleutians. The relations between M_o and M_S obtained by Geller (dashed lines); that is $\log M_o \sim M_S$ for $M_S < 6.76$ and $\log M_o \sim 3/2\ M_S$ for $6.76 < M_S < 8.12$ are somewhat consistent with our data.

Figure 2 shows the m_b values versus M_S values and compares them with Geller's lines. From the m_b-M_S relation and M_S-M_o relation, we might say the scaling laws relating M_o to m_b and m_b to M_s derived by Geller can be applied to our data.

Figure 3 shows the observed spectra of the earthquakes studied. Figure 4 is the idealized spectra derived from Geller (1976). In general, the shape of our spectra is similar to those. Actually, there are still some differences between them. Their corner period increases with body-wave magnitude, whereas our corner period is constant at about 10 seconds. Also, our intermediate portion decreases with increasing m_b value. Earthquakes 3 and 4 have the same m_b and M_s values but have different shapes. The level of earthquake 1 from observed data seems about 1 log scale unit lower.

REFERENCES

Aki, K. (1967). Scaling law of seismic spectrum, J. Geophys. Res., 72, 1217-1231.

Aki, K. (1972a). Scaling law of earthquake source time function, Geophys. J., 31, 3-25.

Aki, K. (1972b). Earthquake mechanism, Tectonophysics 13, 423-446.

Brune, J.N. (1970). Tectonic stress and the spectra of seismic shear waves from earthquakes, J. Geophys. Res., 78, 4997-5009.

Chinnery, M.A. (1964). The Earth's crust under horizontal shear stress, J. Geophys. Res., 69, 2085-2089.

Chouet, et al., (1978). Regional variation of the scaling law of earthquake source spectrum, Bull. Seism. Soc. Am., 68, 49-80.

Geller, R.J., (1976). Scaling relations for earthquake source functions and magnitude, Bull. Seism. Soc. Am., 66, 1501-1523.

Hanks, T.C. and M. Wyss (1972). The use of body-wave spectra in the determination of seismic-source parameters, Bull. Seism. Soc. Am., 62, 561-589.

Kanamori, H. and D.L. Anderson (1975). Theoretical basis of some empirical relations in seismology, Bull. Seism. Soc. Am., 65, 1073-1095.

Nuttli, O.W. and V.V. Gudaitis (1966). On the amplitudes of long period P waves (abstract), Earthquake Notes, 37, (4) 24.

Stauder, W. (1968). Tensional character of earthquake foci beneath the Aleutian trench with relation to sea-floor spreading, J. Geophys. Res., 73, 7693-7701.

Trifunac, M.D. (1972). Stress estimates for the San Fernando, California earthquake of February 9, 1971, Main event and thirteen aftershocks. Bull. Seism. Soc. Am., 62, 721-751.

Wyss, M. and J.N. Brune (1968). Seismic moment, stress and source dimensions for earthquakes in the California-Nevada region, J. Geophys. Res., 73, 4681-4694.

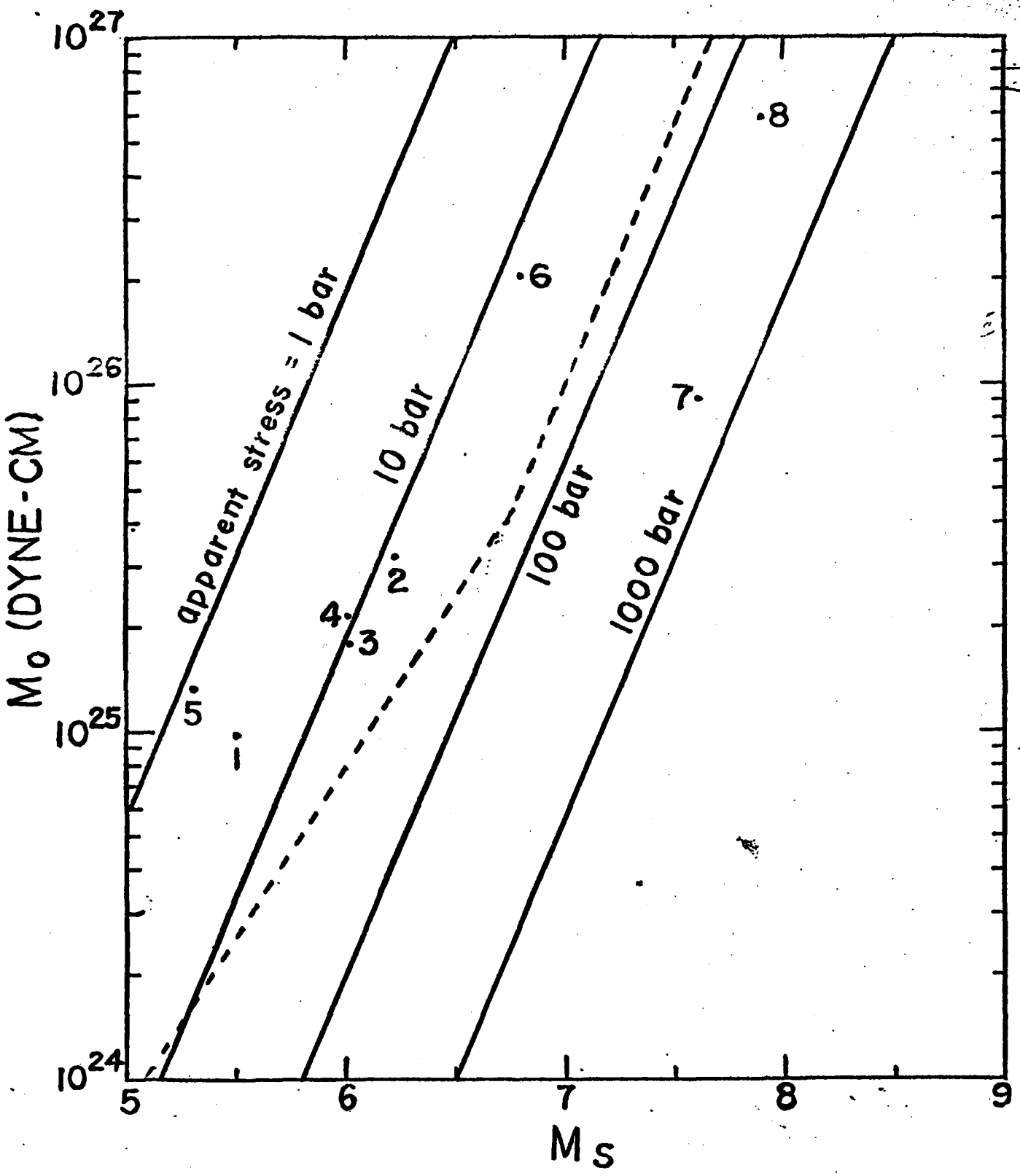

Figure 1. Seismic moment (M_o) versus surface-wave magnitude (M_s). The solid lines are from Kanamori and Anderson (1978). The dashed lines are from Geller (1976).

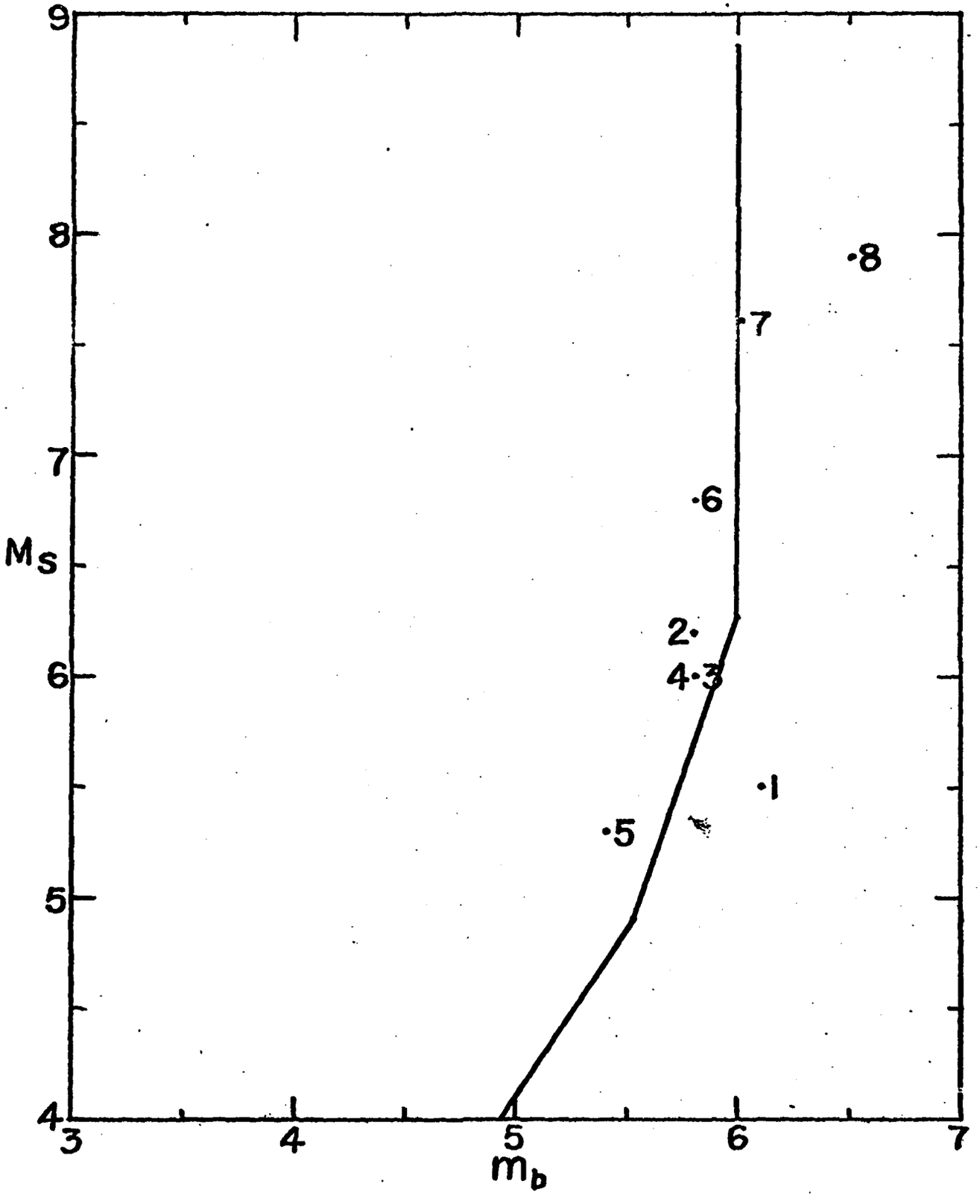

Figure 2. Relation between m_b and M_S. The solid curve is from Geller (1976).

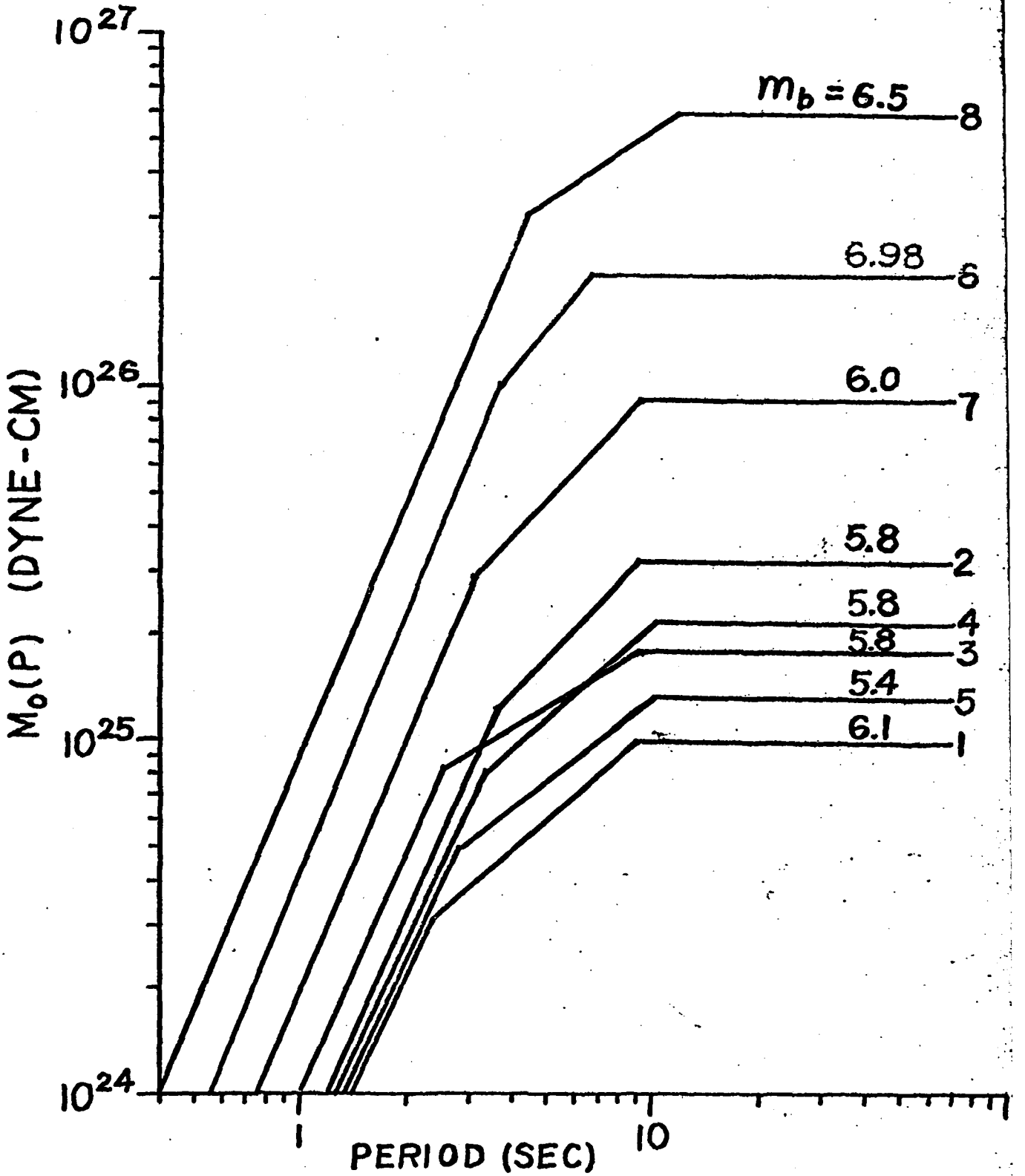

Figure 3. Observed spectra of earthquakes studied.

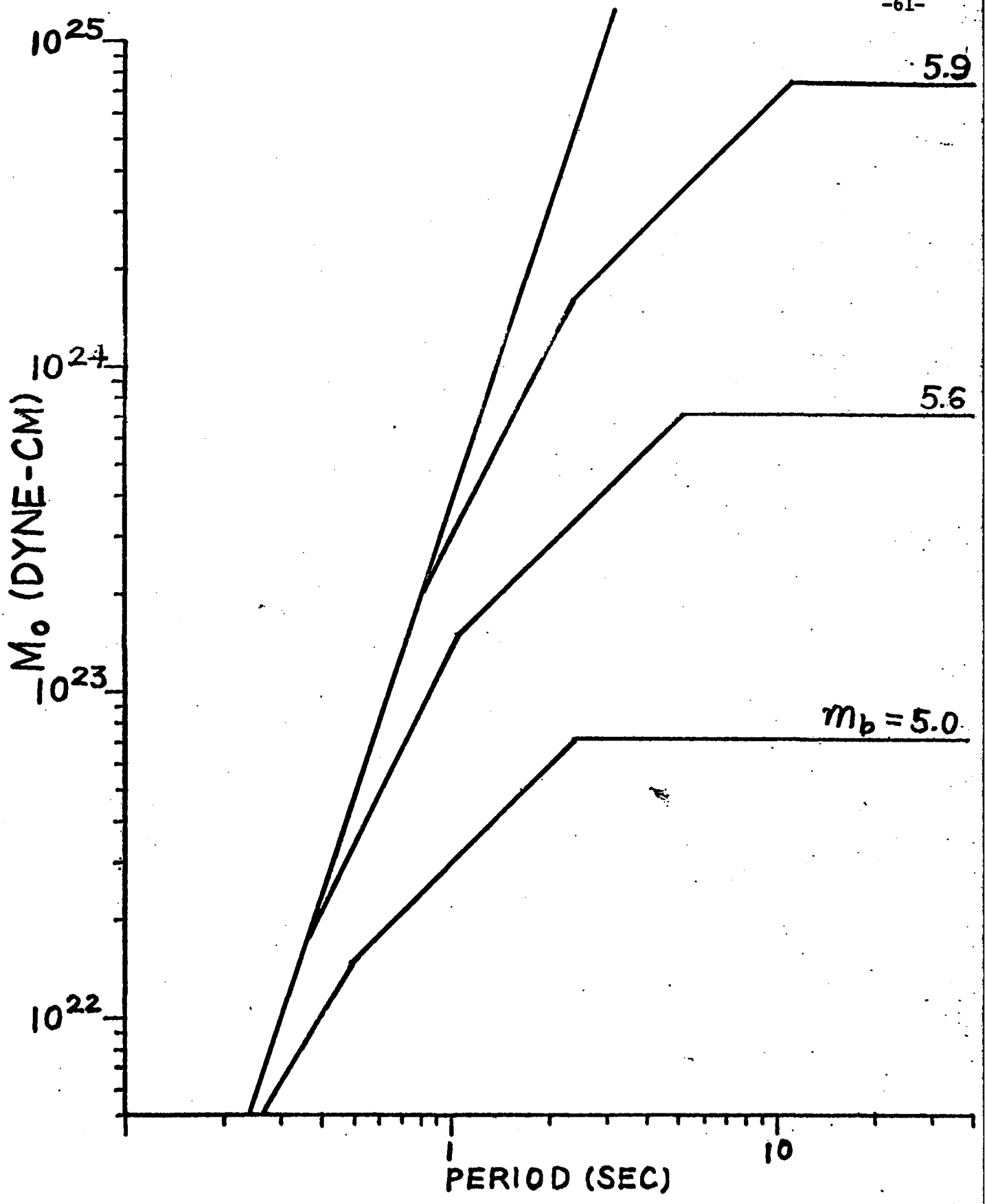

Figure 4(a). Idealized spectra from Geller (1976).

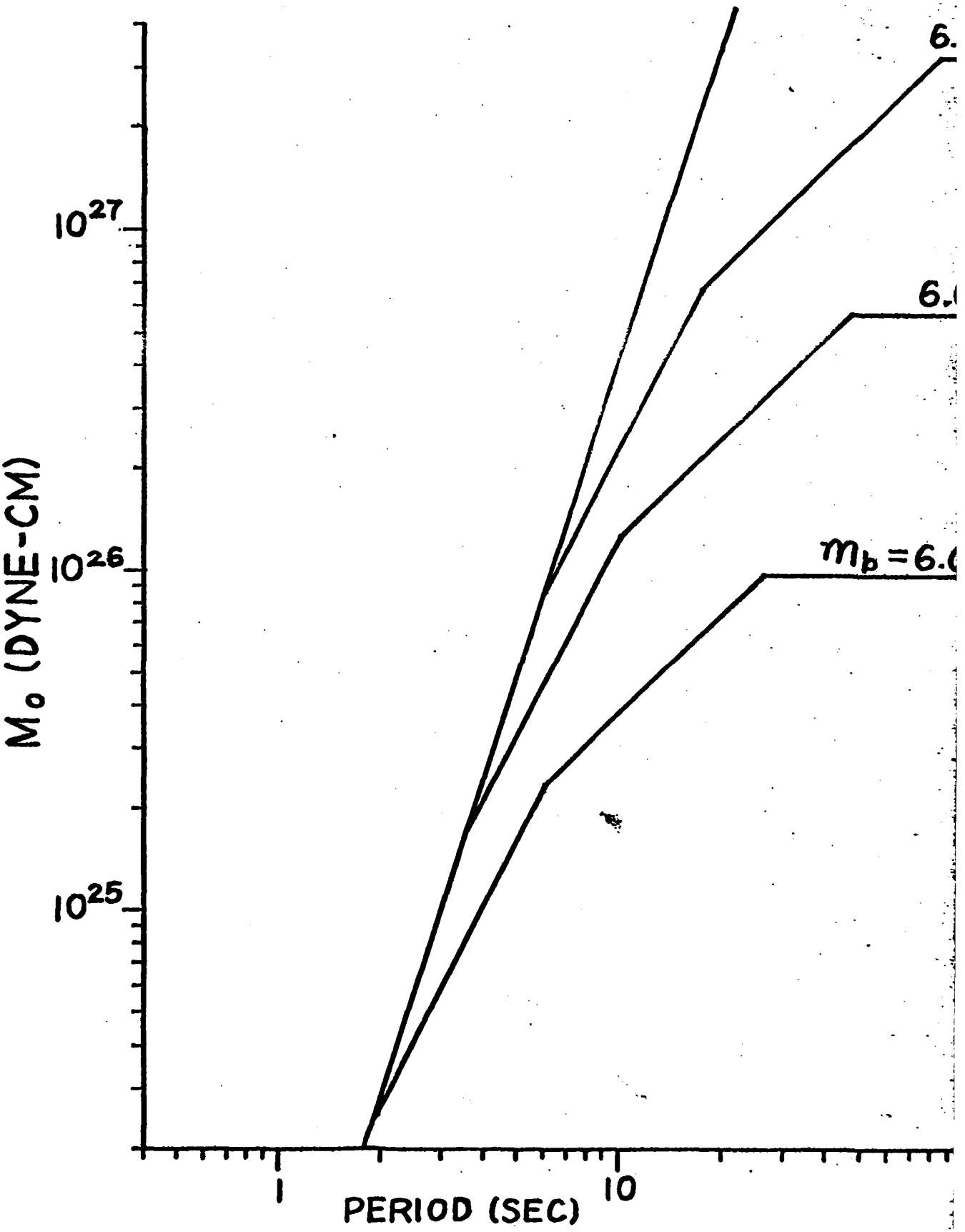

Figure 4(b). Idealized spectra from Geller (1976).